

# Columbia plot based on symmetry-improved CJT formalism in linear sigma model

Yuepeng Guan<sup>1,\*</sup>, Mamiya Kawaguchi<sup>2,†</sup>, Shinya Matsuzaki<sup>1,‡</sup> and Akio Tomiya<sup>3,4,§</sup>

<sup>1</sup>*Center for Theoretical Physics and College of Physics, Jilin University, Changchun, 130012, China*

<sup>2</sup>*Center for Fundamental Physics, School of Mechanics and Physics, Anhui University of Science and Technology, Huainan, Anhui 232001, People's Republic of China*

<sup>3</sup>*Department of Information and Mathematical Sciences,*

*Tokyo Woman's Christian University, Tokyo 167-8585, Japan*

<sup>4</sup>*RIKEN Center for Computational Science, Kobe 650-0047, Japan*

We study the Columbia plot for the chiral phase transition in the framework of a three-flavor linear sigma model based on the Cornwall-Jackiw-Tomboulis (CJT) formalism. The conventional CJT approach with the Hartree truncation suffers from artificial chiral breaking, leading to the violation of the Nambu-Goldstone theorem and the (anomalous) chiral Ward-Takahashi identities. We apply the symmetry-improved CJT formalism to resolve this issue. We observe a first-order phase transition and a tricritical point in the light-quark mass regime, which is fairly insensitive to the size of the sigma meson, in contrast to the conventional CJT approach. The tricritical point, found on the  $m_s$  axis, is at  $m_s^{\text{tri}}/m_s^{\text{phys.}} = 0.175$  with  $m_s^{\text{phys.}}$  being the physical strange quark mass in real-life QCD. The critical pion mass in the three-flavor symmetric limit, on the second-order boundary, is measured at  $m_\pi \sim 52.4$  MeV, with the critical temperature  $T_c \sim 51.7$  MeV.

## I. INTRODUCTION

Quantum Chromodynamics (QCD) exhibits a rich phase structure at high temperature associated with chiral symmetry restoration and deconfinement. Deep understanding of the chiral phase transition is of importance to explore the origin of mass and matter. The study along this line has attracted a growing interest in not only the current terrestrial experiments, but also astrophysical and cosmological observations; heavy-ion collisions [1–4], neutron star interiors [5–7], and the thermal history of the early universe [8, 9].

In the general QCD parameter space, the chiral phase transition can be characterized by the lightest quark mass  $m_u = m_d \equiv m_l$  and the strange quark mass  $m_s$ . The parameter space is called the Columbia plot [10, 11]. The physical point at which QCD of the Standard Model is located, thus, is merely a single point in the continuous quark mass parameter space. Going off the physical point therefore brings a broader and deeper view of how the chiral phase transition, hence the origin of mass and matter, is realized in real-life QCD.

The phase structure of the Columbia plot for the small  $m_l$  regime is still an open question. It is typically classified into three “scenarios” [11–19]:

- i) the *tricritical point* at  $m_s = m_s^{\text{tri}}$  on the  $m_s$ -axis with  $m_u = m_d = 0$  is present, at which point the first order regime is closed and the phase transition becomes second order, which ever persists toward the two-flavor chiral limit,  $m_s \rightarrow \infty$ , reflecting the universality class of the  $O(4)$  theory with no  $U(1)$  axial symmetry restoration;
- ii) the tricritical point is absent and  $U(1)$  axial symmetry is restored; hence, that is not in the  $O(4)$  universality class, so that the first-order regime can be observed till the two-flavor chiral limit;
- iii) no first-order regime emerges and the second-order regime shows up only on the  $m_s$ -axis.

Upon the current status of the lattice simulations, for  $2 + 1$  flavor QCD with small  $m_l$  and large  $m_s$ , either scenarios i) or ii) tend to be favored [20–28]. The functional renormalization group (fRG) approach to QCD has also realized scenario i) for the two-flavor [29] and  $2 + 1$ -flavor cases [30]. In the three-flavor symmetric case with  $m_l = m_s$ , Scenario iii) has been supported [14–16, 31, 32]. The first-order signal has not yet been observed even for a small pion mass, down to  $m_\pi \lesssim 50$  MeV with highly improved staggered fermions [14, 31] and  $m_\pi \lesssim 110$  MeV with improved Wilson fermions [32]. A recent analysis using the Dyson-Schwinger equation has also supported a second-order phase transition for three massless quark flavors [17], namely, implying no first-order regime in the small-quark mass regime.

Alternatively to lattice QCD studies, low-energy effective field theories (LEFTs) can also provide a complementary view of the investigation on the chiral phase structure on the Columbia plot [12, 33–47]. These theories qualitatively

\* guanyp22@mails.jlu.edu.cn

† mamiya@aust.edu.cn

‡ synya@jlu.edu.cn

§ akio@yukawa.kyoto-u.ac.jp

capture the relevant infrared dynamics through effective degrees of freedom (light mesons and quarks), keeping the global symmetries such as the chiral symmetry and its violation characteristic proper in QCD. The linear sigma model (LSM) is one candidate description as such, which serves as a particularly valuable framework for studying chiral phase transitions.

In employing the LSM, one notices one remark made in the literature [12], showing that fluctuations like mesonic loop corrections substantially modify the result in the mean-field approximation projected onto the Columbia plot. To properly incorporate the potentially nonperturbative mesonic loop corrections, one can use the Cornwall-Jackiw-Tomboulis (CJT) method in two-particle (2PI) irreducible effective action formulations. Plugging this formalism into an LSM, one will solve the gap equation for two-point functions of meson fields which involve resummed nonperturbative propagators. Accordingly, the nonperturbative vacuum will be determined at the stationary point for not only the chiral-order parameter but also the meson propagators. This formalism would thus provide an alternative approach to nonperturbatively study the Columbia plot based on a different systematics compared to other nonperturbative methods, such as the fRG and Dyson-Schwinger equations, and also lattice simulations.

However, it has also been pointed out that the CJT method inevitably suffers from the difficulty that the Nambu-Goldstone (NG) theorem or the threshold property at the criticality are violated [33, 35, 48]. This is because a non-systematic truncation of the 2PI digrams, e.g., often referred to as the Hartree approximation, is required to apply in practically evaluating the CJT effective action at the two-loop level; hence non-chiral invariant set of the two-loop corrections generates artificial chiral breaking, which feeds back to the violent deviation from the low-energy theorem and the NG theorem in the chiral limit as well. This issue is therefore crucial around the criticality of the chiral phase transition. In fact, the violation of the NG theorem is reflected in generating the massive NG boson at finite temperature even in the case without the explicit symmetry breaking (e.g. the chiral limit for the QCD case). In the literature [48], it has been clarified that the loopwise truncation deviates the Ward-Takahashi identities (WTIs) between the one-particle irreducible (1PI) and the 2PI actions, with the former protecting the NG theorem at any order of truncation.

Thus, the so-called *symmetry-improved (SI) CJT* formalism has been proposed with the enforcement of the 1PI WTIs to preserve the original global symmetry ( $O(N)$  symmetry as a reference model) [48]. An application of this original SICJT formalism to  $O(4)$  LSM has been performed in [49], where the two-flavor chiral phase transition has been addressed in the chiral limit with the exact NG boson even at finite temperature.

In this paper, we apply the SICJT formalism to a three-flavor LSM and explore the chiral phase structure in the small-quark mass regime of the Columbia plot. We observe a first-order regime and a tricritical point consistently with Scenario i) above. This is a definitive conclusion fairly insensitive to the size of the sigma meson mass, in contrast to the conventional CJT approach in [33, 35].

This paper is organized as follows. In Sec. II, we introduce a three-flavor LSM and summarize what is necessary to address the chiral phase transition in the CJT formalism at zero and finite temperature. This section is essentially just a review of the literature [33, 35, 50]. In Sec. III, applying the argument in [48] to the present LSM case, we discuss the violation of the NG theorem by demonstrating the discrepancy between the WTIs associated with the 1PI and the 2PI formalisms. Then, we introduce the SICJT formulation established in [48]. In Sec. IV, we show our results on the chiral phase transitions and projection onto the Columbia plot, and discuss the related physical consequences, in comparison with the results based on the conventional CJT approach. The conclusion of this paper is provided in Sec. V. In Appendices A, B, C, and D, we also present supplementary materials for more details relevant to the present work: tree-level formulae in the LSM (A); the CJT formalism (B); the WTIs with and without explicit breaking (C); the criticalities seen in the Columbia plots (D).

## II. AN LSM AND CJT FORMALISM

We begin by introducing a phenomenologically successful three-flavor LSM proposed in [51] and analyzed at finite temperature in [50] within the conventional CJT formalism [52]. This LSM can, in particular, reproduce what is called the inverse mass hierarchy between  $a_0(950)$  and  $\kappa(700) = K_0^*(700)$  spectra, due to the introduction of the explicit-chiral breaking contribution related to the  $U(1)$ -axial anomaly-induced term (see Eq.(8)) [51]. Some of the detailed formulae can be found in Appendices A and B.

The central building block of the model is the LSM field  $\Phi$ , which transforms bifundamentally under the full  $U(3)_L \times U(3)_R$  symmetry as

$$\Phi \rightarrow g_L \cdot \Phi \cdot g_R^\dagger, \quad (1)$$

with  $g_{L,R} \in U(3)_{L,R}$ . Throughout the present paper, we work in Euclidean spacetime. The model Lagrangian is given

as

$$\mathcal{L}_{\text{LSM}} = \text{tr} \left[ \partial_\mu \Phi^\dagger \partial_\mu \Phi \right] + V(\Phi, \Phi^\dagger), \quad (2)$$

The mesonic field  $\Phi$  is parametrized as  $\Phi = \phi_a T^a = (\sigma_a + i\pi_a) T^a$  for  $a = 0, \dots, 8$ , in which  $\sigma_a$  and  $\pi_a$  denote the scalar and pseudoscalar fields, respectively.  $T^a = \lambda^a/2$  represents generators of the  $U(3)$  group, in which  $\lambda^{a=1, \dots, 8}$  are the Gell-Mann matrices, and  $\lambda^0 = \sqrt{2/3} \mathbf{1}_{3 \times 3}$ . The mesonic potential  $V(\Phi, \Phi^\dagger)$  in Eq. (2) is given by

$$V(\Phi, \Phi^\dagger) = V_0 + V_{\text{anom}} + V_{\text{SB}} + V_{\text{SB-anom}}. \quad (3)$$

The first term  $V_0$  in Eq.(3) corresponds to the  $U(3)_L \times U(3)_R$  invariant part. This potential term is, up to mass dimension four, given as

$$V_0 = \mu^2 \text{tr} [\Phi^\dagger \Phi] + \lambda_1 \text{tr} [(\Phi^\dagger \Phi)^2] + \lambda_2 (\text{tr} [\Phi^\dagger \Phi])^2. \quad (4)$$

The second term  $V_{\text{anom}}$  in Eq.(3) arises from the QCD instanton contribution associated with the  $U(1)$  axial anomaly. It takes the determinant form, the so-called Kobayashi-Maskawa-'t Hooft (KMT) term [53–56],

$$V_{\text{anom}} = -B(\det [\Phi] + \det [\Phi^\dagger]). \quad (5)$$

The third term  $V_{\text{SB}}$  in Eq.(3) is the leading-order explicit chiral-breaking term tied with the low-energy theorem,

$$V_{\text{SB}} = -c \text{tr} [\mathcal{M} \Phi^\dagger + \mathcal{M}^\dagger \Phi]. \quad (6)$$

Here  $\mathcal{M}$  is the spurion field, which transforms in the same way as  $\Phi$  in Eq.(1),

$$\mathcal{M} \rightarrow g_L \cdot \mathcal{M} \cdot g_R^\dagger, \quad (7)$$

and takes the vacuum expectation value (VEV)  $\mathcal{M} \equiv \text{diag}\{m_u, m_d, m_s\}$  to incorporate the proper explicit-chiral breaking into mesons arising from the current quark masses present in QCD.

The fourth term  $V_{\text{SB-anom}}$  in Eq.(3) is characteristic to the present LSM,

$$V_{\text{SB-anom}} = -kc \left[ \epsilon_{abc} \epsilon^{def} \mathcal{M}_d^a \Phi_e^b \Phi_f^c + \text{h.c.} \right]. \quad (8)$$

This is the axial-anomaly induced flavor-breaking term, which controls the inverse mass hierarchy for  $a_0$  and  $K_0^*$  masses [51].

The dynamical chiral symmetry breaking is monitored by the chiral order parameter, i.e., the VEV, or the thermal average of  $\Phi$ , which is parameterized as

$$\langle \Phi \rangle \equiv \bar{\Phi} = \bar{\sigma}_a T^a, \quad (9)$$

without loss of generality. The isospin symmetry is adopted as  $m_u = m_d \equiv m_l \neq m_s$ , such that the VEVs of the  $\sigma$ -fields read

$$\bar{\sigma}_a T^a = \bar{\sigma}_0 T^0 + \bar{\sigma}_8 T^8 = \text{diag}\{\bar{\Phi}_1, \bar{\Phi}_1, \bar{\Phi}_3\}, \quad (10)$$

together with the following relations:

$$\begin{aligned} \bar{\Phi}_1 &= \frac{1}{\sqrt{6}} \bar{\sigma}_0 + \frac{1}{2\sqrt{3}} \bar{\sigma}_8, \\ \bar{\Phi}_3 &= \frac{1}{\sqrt{6}} \bar{\sigma}_0 - \frac{1}{\sqrt{3}} \bar{\sigma}_8. \end{aligned} \quad (11)$$

At tree-level, the stationary condition reads

$$\left. \frac{\delta S_{\text{LSM}}}{\delta \Phi_1} \right|_{\Phi=\bar{\Phi}} = 0, \quad \left. \frac{\delta S_{\text{LSM}}}{\delta \Phi_3} \right|_{\Phi=\bar{\Phi}} = 0, \quad (12)$$

where  $S_{\text{LSM}} = \int_x \mathcal{L}_{\text{LSM}}$  is the Euclidean action, with the shorthand notation  $\int_x \equiv \int d\tau \int d^3\mathbf{x}$ . The meson mass matrices are given by

$$\begin{aligned} \left[ m_S^2(\bar{\sigma}) \right]^{ab} &= \left. \frac{\partial^2 V_{\text{LSM}}}{\partial \sigma_a \partial \sigma_b} \right|_{\sigma_a = \bar{\sigma}_a}, \\ \left[ m_P^2(\bar{\sigma}) \right]^{ab} &= \left. \frac{\partial^2 V_{\text{LSM}}}{\partial \pi_a \partial \pi_b} \right|_{\sigma_a = \bar{\sigma}_a}. \end{aligned} \quad (13)$$

The explicit expressions and derivations for those formulae can be found in Appendix A. For the scalar mesons,  $\left[ m_S^2(\bar{\sigma}) \right]^{11}$  are  $\left[ m_S^2(\bar{\sigma}) \right]^{44}$  respectively identified as the squared masses for  $a_0(980)$ ,  $m_{a_0}^2$ , and  $\kappa(700) = K_0^*(700)$ ,  $m_\kappa^2$ . The  $f_0(500)$  and  $f_0(980)$  masses arise as the mass eigenvalues from the isospin-singlet scalar mass matrix through a mixing angle  $\theta_S^0$  defined with an orthogonal transformation matrix in Eq. (A14). Similarly to the scalar mesons,  $\left[ m_P^2(\bar{\sigma}) \right]^{11} = m_\pi^2$  and  $\left[ m_P^2(\bar{\sigma}) \right]^{44} = m_K^2$ , respectively. The  $\eta'$  and  $\eta$  masses are read as the mass eigenvalues for the isospin-singlet pseudoscalar-mass matrix with a mixing angle  $\theta_P^0$ , as in Eq. (A19).

To evaluate the quantum and thermal corrections arising in the present LSM at finite temperature  $T$ , we apply the CJT formalism [52]. We start from the general loop expansion of the 2PI effective potential for the LSM with  $N_f$  flavors, which goes like

$$\begin{aligned} &V_{\text{CJT}}[\sigma, S, P] \\ &= V(\sigma) + \frac{1}{2} \int_k \text{tr} \left[ \log S^{-1}(k) + \log P^{-1}(k) \right] \\ &\quad + \frac{1}{2} \int_k \text{tr} \left[ \bar{S}^{-1}(k; \sigma) S(k) + \bar{P}^{-1}(k; \sigma) P(k) - 2 \cdot \mathbf{1}_{\text{adj}} \right] \\ &\quad + V_2[\sigma, S, P], \end{aligned} \quad (14)$$

where  $\sigma$  is a general background field; the trace is taken in the flavor space;  $V(\sigma)$  is the tree-level potential defined in Eq. (3), and  $V_2[\sigma, S, P]$  is the sum of all 2PI diagrams, which are constructed by the full-meson propagators  $\mathcal{S}$  and  $\mathcal{P}$ ;  $\mathbf{1}_{\text{adj}}$  is the unit matrix in the adjoint representation of  $SU(3)$  having the size of  $N_f^2 \times N_f^2$ ; the full scalar (pseudoscalar) propagators are denoted as  $S$  ( $P$ ), which are treated as independent variables in the present framework. In Eq.(14) we have abbreviated the loop momentum integral as  $\int_k f(k) \equiv T \sum_n \int d^3\mathbf{k} / (2\pi)^3 f(\omega_n, \mathbf{k})$  with  $\omega_n$  being the bosonic Matsubara frequency. In Eq. (14),  $\bar{S}^{-1}(k; \sigma)$  and  $\bar{P}^{-1}(k; \sigma)$  are the tree-level mesonic inverse propagators induced from the tree-level action, which reads

$$\begin{aligned} \left[ \bar{S}^{-1}(k; \sigma) \right]^{ab} &= k^2 \delta^{ab} + \left[ m_S^2(\sigma) \right]^{ab}, \\ \left[ \bar{P}^{-1}(k; \sigma) \right]^{ab} &= k^2 \delta^{ab} + \left[ m_P^2(\sigma) \right]^{ab}. \end{aligned} \quad (15)$$

In the present work, we adopt the Hartree approximation, by which the sum of the 2PI diagram terms  $V_2$  in Eq.(14) is truncated at the two-loop level as follows:

$$\begin{aligned} &V_2[S, P] \\ &= \mathcal{F}^{abcd} \left[ \int_k S_{ab}(k) \int_q S_{cd}(q) + \int_k P_{ab}(k) \int_q P_{cd}(q) \right] \\ &\quad + 2\mathcal{H}^{abcd} \int_k S_{ab}(k) \int_q P_{cd}(q), \end{aligned} \quad (16)$$

where  $\mathcal{F}^{abcd}$  and  $\mathcal{H}^{abcd}$  are associated with the four-meson couplings  $\lambda_1$  and  $\lambda_2$  in Eq.(4), and the explicit expressions are given in Eq. (B8). The corresponding Feynman diagrams are illustrated in Fig. 1. In the current setup, the daisy-type diagrams are resummed systematically by solving the gap equation of the meson propagators (see also Eq. (20)).

The nonperturbative VEVs (or the thermal averages) of  $\sigma_a$  and the full scalar and pseudoscalar meson propagators

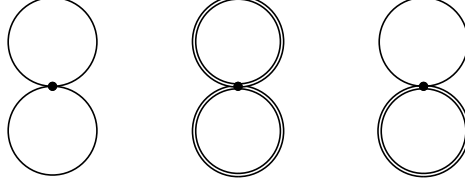


FIG. 1. Feynman diagrams in the Hartree approximation contributing to  $V_2$  in Eq. (B7). The solid lines represent the scalar meson propagators  $S_{ab}$ , and the doubled solid lines the pseudoscalar meson propagators  $P_{ab}$ . The black blob stands for the bare vertices, which are denoted in the text as  $\mathcal{F}^{abcd}$  and  $\mathcal{H}^{abcd}$ , respectively.

$S_{ab}$  and  $P_{ab}$  are determined by the stationary condition for  $V_{\text{CJT}}$  at  $\sigma = \bar{\sigma}$ ,  $S = \mathcal{S}$ , and  $P = \mathcal{P}$  as

$$\begin{aligned} \left. \frac{\partial V_{\text{CJT}}[\sigma, S, P]}{\partial \sigma_a} \right|_{\sigma=\bar{\sigma}, S=\mathcal{S}, P=\mathcal{P}} &= 0, \\ \left. \frac{\delta V_{\text{CJT}}[\sigma, S, P]}{\delta S_{ab}} \right|_{\sigma=\bar{\sigma}, S=\mathcal{S}, P=\mathcal{P}} &= 0, \\ \left. \frac{\delta V_{\text{CJT}}[\sigma, S, P]}{\delta P_{ab}} \right|_{\sigma=\bar{\sigma}, S=\mathcal{S}, P=\mathcal{P}} &= 0. \end{aligned} \quad (17)$$

See also Eq.(B5). In the Hartree approximation, as evident from Fig. 1, the loop corrections are all contact such that no external momentum dependence is renormalized from the tree-level one for meson-two point functions. Therefore, we parameterize the nontrivial solution for (inverse) meson propagators,  $\mathcal{S}_{ab}$  and  $\mathcal{P}_{ab}$ , only with momentum-independent dynamical mass terms as follows:

$$\begin{aligned} [\mathcal{S}^{-1}(k)]^{ab} &= k^2 \delta^{ab} + [M_S^2]^{ab}, \\ [\mathcal{P}^{-1}(k)]^{ab} &= k^2 \delta^{ab} + [M_P^2]^{ab}. \end{aligned} \quad (18)$$

Then, the stationary condition in Eq. (17) is cast into the form,

$$\begin{aligned} 0 &= \frac{\partial V(\bar{\sigma})}{\partial \bar{\sigma}_0} - 3\mathcal{G}^{0bc} \left[ \int_k \mathcal{S}_{cb}(k) - \int_k \mathcal{P}_{cb}(k) \right] \\ &\quad + 4\mathcal{F}^{0bcd} \bar{\sigma}_b \int_k \mathcal{S}_{dc}(k) + 4\mathcal{H}^{0bcd} \bar{\sigma}_b \int_k \mathcal{P}_{dc}(k), \\ 0 &= \frac{\partial V(\bar{\sigma})}{\partial \bar{\sigma}_8} - 3\mathcal{G}^{8bc} \left[ \int_k \mathcal{S}_{cb}(k) - \int_k \mathcal{P}_{cb}(k) \right] \\ &\quad + 4\mathcal{F}^{8bcd} \bar{\sigma}_b \int_k \mathcal{S}_{dc}(k) + 4\mathcal{H}^{8bcd} \bar{\sigma}_b \int_k \mathcal{P}_{dc}(k), \end{aligned} \quad (19)$$

and

$$\begin{aligned} [M_S^2]^{ab} &= [m_S^2(\bar{\sigma})]^{ab} \\ &\quad + 4\mathcal{F}^{abcd} \int_k \mathcal{S}_{cd}(k) + 4\mathcal{H}^{abcd} \int_k \mathcal{P}_{cd}(k), \\ [M_P^2]^{ab} &= [m_P^2(\bar{\sigma})]^{ab} \\ &\quad + 4\mathcal{F}^{abcd} \int_k \mathcal{P}_{cd}(k) + 4\mathcal{H}^{abcd} \int_k \mathcal{S}_{cd}(k). \end{aligned} \quad (20)$$

The detailed expression of  $\mathcal{G}^{abc}$ , which has been introduced in Eq.(19) is given in Eq. (B26), which is associated with the  $U(1)$  axial anomaly, i.e. the KMT determinant term proportional to  $B$  in Eq.(5).

### III. (ANOMALOUS) WTIS VERSUS 2PI FORMALISM: LOAD TO SICJT

In this section, following [48], we review the intrinsic issue of the 2PI formalism on the violation of the NG theorem and the (anomalous) WTIs. For readability, we will pick up only the resultant key equations and the detailed derivations of the WTIs are referred to as in Appendix C.

Consider an action  $S[\phi]$  having a symmetry associated with the infinitesimal transformation of a set of general field  $\phi_a$  ( $a = 1, \dots$ ) as  $\phi_a \rightarrow \phi_a + i\epsilon\delta_\epsilon\phi_a$ , where  $\delta_\epsilon\phi_a$  is the corresponding generator in the field space. Momentarily, no explicit breaking is assumed for the original symmetry. Through the symmetry transformation of the generating functional (with the source  $J^a$ ), we have the following WIT

$$J^a \cdot \langle \delta_\epsilon\phi_a \rangle_J = 0. \quad (21)$$

If the generator belongs to the linear symmetry representation in the corresponding Lie group, such as  $\delta_\epsilon\phi_a = d_a^b\phi_b$  with  $d$  being an arbitrary coefficient matrix, we then get the following WTI for the 1PI effective action  $\Gamma$ :

$$\frac{\delta\Gamma}{\delta(\phi_{\text{cl}})_a} \cdot \delta_\epsilon(\phi_{\text{cl}})_a = 0, \quad (22)$$

where  $(\phi_{\text{cl}})_a \equiv \langle \phi_a \rangle_J$  is the VEV including the source field  $J$ .

In the case of the chiral- $SU(3)$  transformation given in Eq.(1), we find

$$\delta^\alpha\sigma_a = d^{\alpha b}{}_a\pi_b, \quad \delta^\alpha\pi_a = -d^{\alpha b}{}_a\sigma_b, \quad (23)$$

Following Eq.(22), in the case without explicit breaking, i.e., in the three-flavor chiral limit, the WTIs for these chiral rotations are then read off as

$$\frac{\delta\Gamma[\sigma_{\text{cl}}, \pi_{\text{cl}}]}{\delta(\sigma_{\text{cl}})_a} \cdot d^{\alpha b}{}_a(\pi_{\text{cl}})_b + \frac{\delta\Gamma[\sigma_{\text{cl}}, \pi_{\text{cl}}]}{\delta(\pi_{\text{cl}})_a} \cdot d^{\alpha b}{}_a(\sigma_{\text{cl}})_b = 0. \quad (24)$$

Passing through a couple of algebraic computations (see Appendix C), Eq.(24) can finally be reduced to the following simple relations:

$$M_\pi^2\bar{\Phi}_1 = 0, \quad M_K^2(\bar{\Phi}_1 + \bar{\Phi}_3) = 0, \quad (25)$$

where we have also used Eq.(11). The  $M_\pi$  and  $M_K$  denote the full nonperturbative pion and kaon masses arising from the full propagator  $P_{ab}$ . Equation (25) manifests itself that in the chiral limit, the spontaneously chiral broken phase with  $\bar{\Phi}_1 \neq 0$  or  $\bar{\Phi}_3 \neq 0$  yields  $M_\pi = 0$  and  $M_K = 0$ , precisely reflecting the NG theorem. The chiral-limit WTI only for the two-flavor chiral rotation has been discussed in [49], which has been currently extended by including the  $M_K$  term in Eq.(25).

The above formulations can be further generalized to the case with explicit chiral symmetry breaking supplied from the spurion field for the current quark masses,  $\mathcal{M}$ . The action  $S$ , corresponding to the LSM Lagrangian (2), is  $SU(3)$  chiral invariant by including the (infinitesimal) transformation of  $\mathcal{M}$  given in Eq.(7) together with Eq.(23). The WTIs (22) are then generalized into the so-called anomalous chiral WTIs [57, 58]:

$$\left\langle \frac{\delta S}{\delta \mathcal{M}} \right\rangle_J \cdot \delta_\epsilon \mathcal{M} + \left\langle \frac{\delta S}{\delta \mathcal{M}^\dagger} \right\rangle_J \cdot \delta_\epsilon \mathcal{M}^\dagger + J^a \cdot \langle \delta_\epsilon\phi_a \rangle_J = 0. \quad (26)$$

After somewhat lengthy calculations (see Appendix C), we see that Eq.(26) gives a naturally extended formulae in the presence of the current quark masses for  $M_\pi$  and  $M_K$  from the chiral limit case in Eq.(25):

$$M_\pi^2\bar{\Phi}_1 = cm_l(1 + 2k\bar{\Phi}_3), \\ M_K^2(\bar{\Phi}_1 + \bar{\Phi}_3) = (cm_l + cm_s)(1 + 2k\bar{\Phi}_1). \quad (27)$$

To see the more physical consequences of the constraint relations in Eq.(27), we shall read the light and strange quark condensates, defined as the response of the light and strange quark masses, from the LSM Lagrangian in Eq.(2) as

$$\langle \bar{\ell}\ell \rangle = \left\langle \frac{\partial \mathcal{L}_{\text{LSM}}}{\partial m_l} \right\rangle = -2c(\bar{\Phi}_1 + 2k\bar{\Phi}_1\bar{\Phi}_3), \\ \langle \bar{s}s \rangle = \left\langle \frac{\partial \mathcal{L}_{\text{LSM}}}{\partial m_s} \right\rangle = -2c(\bar{\Phi}_3 + 2k\bar{\Phi}_1^2). \quad (28)$$

We also read the pion and kaon decay constants  $f_\pi$  and  $f_K$ , which arise as the overlap amplitudes between the corresponding axialvector currents and pseudoscalars, as

$$\begin{aligned} f_\pi &= 2\bar{\Phi}_1, \\ f_K &= \bar{\Phi}_1 + \bar{\Phi}_3. \end{aligned} \quad (29)$$

From these, we find that two constraint relations in Eq.(27) takes the

$$\begin{aligned} f_\pi^2 m_\pi^2 &= -2m_l \langle \bar{l}l \rangle, \\ f_K^2 m_K^2 &= -\frac{m_l + m_s}{2} (\langle \bar{l}l \rangle + \langle \bar{s}s \rangle), \end{aligned} \quad (30)$$

which are precisely the Gell-Mann-Oakes-Renner (GOR) relations. Note an accidental cancellation of the  $k$  dependence arising from both quark condensates and pion, kaon masses. Thus, the low-energy theorem is intact even in the presence of the intrinsically flavor-violating  $k$ -term [50, 51].

The *threshold property* of the (pseudo) NG bosons at the chiral criticality ( $\bar{\Phi}_{1,3} \rightarrow 0$ ) is thus described by the anomalous WTIs in 1PI formalism. The masses of the NG modes are constrained to zero in the chiral broken phase ( $\bar{\Phi}_1 \neq 0$ ,  $\bar{\Phi}_3 \neq 0$ ), or proportional to the explicit breaking current masses. Since the relations (25) or (27) hold before performing the loop expansion in the 1PI effective action, we expect that the threshold property holds even when we truncate the 1PI effective action loopwise. Hereafter, we shall call both the anomalous chiral WTIs and the chiral-limit WTIs simply the WTIs, otherwise specialized.

Examining the WTIs derived in the 2PI formalism, however, we realize that the situation would be drastically changed. In the chiral limit, the WTIs for the 2PI effective action read

$$\begin{aligned} 0 &= \frac{\delta\Gamma[\phi_{\text{cl}}, \Delta]}{\delta(\phi_{\text{cl}})_a} \cdot d_a^b (\phi_{\text{cl}})_b \\ &\quad + \frac{\delta\Gamma[\phi_{\text{cl}}, \Delta]}{\delta\Delta_{ab}} \cdot (d_b^c \Delta_{ac} + d_a^c \Delta_{cb}), \end{aligned} \quad (31)$$

which leads to the second derivatives;

$$\begin{aligned} 0 &= \frac{\delta^2\Gamma[\phi_{\text{cl}}, \Delta]}{\delta(\phi_{\text{cl}})_c \delta(\phi_{\text{cl}})_a} \cdot d_a^b (\phi_{\text{cl}})_b + \frac{\delta\Gamma[\phi_{\text{cl}}, \Delta]}{\delta(\phi_{\text{cl}})_a} \cdot d_a^c \\ &\quad + \frac{\delta^2\Gamma[\phi_{\text{cl}}, \Delta]}{\delta(\phi_{\text{cl}})_c \delta\Delta_{ab}} \cdot (d_b^c \Delta_{ac} + d_a^c \Delta_{cb}). \end{aligned} \quad (32)$$

Due to the third term appearing in the second line of Eq. (32), this identity does not provide a direct constraint to prevent the NG boson from being massive. If the 1PI and 2PI effective actions are evaluated exactly without any truncation, the solutions of  $\phi_{\text{cl}}^a$  and the propagators  $\Delta_{ab}$  should be the same since they come from the same sourceless generating functional. In this case, the WTIs in the 1PI formalism (e.g., Eq. (26) without  $\mathcal{M}$ -term) and the one in the 2PI formalism (31) should be satisfied simultaneously at the solution to the stationary condition. However, truncating both effective actions at the loop level ( $\Gamma_{\text{tr}}^{1\text{PI}}$  and  $\Gamma_{\text{tr}}^{2\text{PI}}$ ), we find that they will follow different WTIs. Then, since the 2PI WTI does not directly constrain the NG boson mass, the threshold property or the NG theorem would be violated. The schematic sketch of the above scenario is shown in Fig. 2. This issue would be crucial near the criticality of the system, since the massless nature is directly connected to the scale-invariance of the correlators.

To resolve this issue, we employ the SICJT formalism [48], for which the strategy is to replace the stationary condition in Eq.(19) by the generalized GOR relation in Eq.(27) derived from the WTIs of the 1PI formalism, while keeping the second constraint with the gap equations for meson masses in Eq.(20). The solution found in this procedure is denoted as  $\Gamma_{\text{tr}}^{\text{SICJT}}$  in Fig. 2. This completes the current formulation, and we shall apply this method to study the Columbia plot.

#### IV. NUMERICAL ANALYSIS

In this section, we show our numerical results on the  $T$ -dependences for the chiral order parameters, masses of scalar and pseudoscalar meson nonets, by solving the gap equations of the meson propagators in Eq. (20) coupled with the generalized GOR relations in Eq. (27) based on the SICJT formalism. The analysis is performed both at the physical point and in the chiral limit. We then discuss the Columbia plot and make a comparison with the results based on



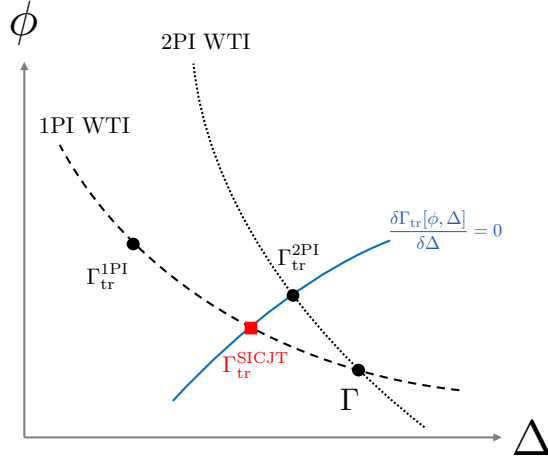


FIG. 2. A schematic sketch of the SICJT formalism. The figure is drawn in the  $(\phi, \Delta)$ -plane where  $\phi$  is the sourced field VEV and  $\Delta$  denotes the sourced propagator, describing the variables of the effective actions. The black blobs (from right to left) represent the solution obtained from the full-quantum action  $\Gamma$ , the truncated 1PI effective action  $\Gamma_{\text{tr}}^{1\text{PI}}$ , and the truncated 2PI effective action  $\Gamma_{\text{tr}}^{2\text{PI}}$ . The black-dashed and -dotted curve respectively denote the constraint trajectories from the 1PI or the 2PI formalism, and the blue-solid line denotes the gap equation of the propagators  $\Delta$  with arbitrary  $\phi$ . The red square mark points to the solution realized by the SICJT formalism.

the conventional CJT formalism, which follows by solving the gap equations coupled to the stationary conditions in Eq. (19), which significantly breaks the NG theorem and threshold property fixed as in the generalized GOR relations in Eq.(27). The criticalities at the tricritical point and the second-order phase boundary, as well as the critical pion mass in the three-flavor symmetric limit, are also addressed in depth.

### A. Numerical implements

Before presenting our results, we briefly summarize the numerical strategy applied in the current work. To solve the coupled equations, we shall adapt the iteration method and decompose the problem into three layers to gain better numerical stability. Given a set of test values for the VEVs  $\Phi_{1,3}$  and full meson masses  $M_{S,P}$ , we fix the values of the mixing angles  $\theta_{S,P}$  through Eq. (B22), by using the Newtonian iteration method with  $\theta_{S,P}^0$  in Eqs.(A15) and (A20) used as initial conditions. Then we solve the gap equations (20) using the fixed-point iteration method with the tree-level masses  $m_{S,P}$ , which can be found in Appendix A 1, used as the initial conditions. Finally, we solve either the stationary condition in Eq. (19) or the GOR relations in Eq (27) by using the Newtonian method with tests of different initial guesses, to search for different phases at a given temperature.

### B. Parameter setup at physical point

We take two different sets of model parameters, characterized by different  $f_0(500)$  mass as an input, to examine the sensitivity of the size of the  $f_0(500)$  mass to the order of phase transition or the phase structure of the Columbia plots, as was discussed earlier [33, 35] based on the conventional CJT formalism.

#### 1. Parameter set I

The first set of parameters is chosen following the literature [50, 51] as

$$\begin{aligned}
 \mu^2 &= 1.02 \times 10^4 \text{ MeV}^2, \quad \lambda_1 = 11.8, \quad \lambda_2 = 20.4, \\
 cm_l^{\text{phys.}} &= 6.11 \times 10^5 \text{ MeV}^3, \\
 cm_s^{\text{phys.}} &= 198 \times 10^5 \text{ MeV}^3, \\
 B &= 3.85 \times 10^3 \text{ MeV}, \quad k = 3.40 \times 10^{-3} \text{ MeV}^{-1},
 \end{aligned} \tag{33}$$



which provides the pion and kaon decay constants as  $f_\pi = 92.1$  MeV and  $f_K = 109.8$  MeV in Eq.(29), and the meson mass spectra

$$\begin{aligned} m[f_0(500)] &= 672.4 \text{ MeV}, & m[f_0(980)] &= 990.4 \text{ MeV}, \\ m_{a_0} &= 937.6 \text{ MeV}, & m_\kappa &= 863.4 \text{ MeV}, \\ m_{\eta'} &= 958.2 \text{ MeV}, & m_\eta &= 552.9 \text{ MeV}, \\ m_\pi &= 137.9 \text{ MeV}, & m_K &= 494.1 \text{ MeV}. \end{aligned} \quad (34)$$

The mixing angles at vacuum are

$$\theta_S^0 = 44.3^\circ, \quad \theta_P^0 = 6.80^\circ. \quad (35)$$

## 2. Parameter set II

We re-fit the parameters following the  $\chi^2$ -fit procedure as performed in Ref. [51], with replacing the  $f_0(500)$  mass by  $m[f_0(500)] = 800$  MeV. Then we get the following best-fit values for the model parameters:

$$\begin{aligned} \mu^2 &= -1.79 \times 10^5 \text{ MeV}^2, & \lambda_1 &= 30.9, & \lambda_2 &= 22.2, \\ cm_l^{\text{phys.}} &= 6.11 \times 10^5 \text{ MeV}^3, \\ cm_s^{\text{phys.}} &= 198 \times 10^5 \text{ MeV}^3, \\ B &= 3.86 \times 10^3 \text{ MeV}, & k &= 1.51 \times 10^{-3} \text{ MeV}^{-1}, \end{aligned} \quad (36)$$

which provides the pion and kaon decay constants as  $f_\pi = 92.1$  MeV and  $f_K = 109.8$  MeV, and the meson mass spectra

$$\begin{aligned} m[f_0(500)] &= 797.1 \text{ MeV}, & m[f_0(980)] &= 1151 \text{ MeV}, \\ m_{a_0} &= 943.1 \text{ MeV}, & m_\kappa &= 966.5 \text{ MeV}, \\ m_{\eta'} &= 897.0 \text{ MeV}, & m_\eta &= 513.9 \text{ MeV}, \\ m_\pi &= 125.8 \text{ MeV}, & m_K &= 460.1 \text{ MeV}. \end{aligned} \quad (37)$$

The mixing angles at vacuum are

$$\theta_S^0 = 45.0^\circ, \quad \theta_P^0 = 0.291^\circ. \quad (38)$$

Notice that the physical observables obviously deviate from the inputs, which indicates that the current parameter space may not fully cover the input observables.

## C. Chiral phase transition at physical point

In Fig. 3 we show the  $T$ -dependences on  $\bar{\Phi}_{1,3}$ , and the scalar and pseudoscalar meson masses  $M_S$  and  $M_P$  at the physical point  $(m_l, m_s) = (m_l^{\text{phys.}}, m_s^{\text{phys.}})$  with the parameter set I provided in Sec. IV B 1. In the figure, the upper panel refers to the conventional CJT method, while the lower panel corresponds to the result from the SICJT method. Comparing both methods, we find the following qualitative characteristics:

- The pseudocritical temperature of the light quark condensate,  $T_{\text{pc}}$ , which is defined by the temperature with the maximum thermal susceptibility  $\chi_T = -\partial\langle\bar{\ell}\ell\rangle_T/\partial T$ , is around  $\sim 185$  MeV in the SICJT formalism, which gets decreased compared to the one from the conventional CJT case with  $T_{\text{pc}} \sim 215$  MeV;
- The pion mass  $M_\pi$  shows relatively smoother  $T$ -dependence for  $T \lesssim T_{\text{pc}}$  in the SICJT formalism, compared to the conventional CJT case. before the chiral restoration happens. This is due to the realization of the proper threshold property and the manifest NG theorem: the introduction of loop corrections in the conventional CJT method breaks the low-energy theorem, i.e., the GOR relations, such that (pseudo) NG boson mass spectra can develop artificially and unphysically with finite  $T$ .

Both cases show the degeneracy of the meson mass spectra at  $T > T_{\text{pc}}$ , which precisely reflects the effective restoration of the chiral symmetry due to the reduction of the size of the light quark condensate. The parameter set II in Sec. IV B 2 yields substantially the same results.

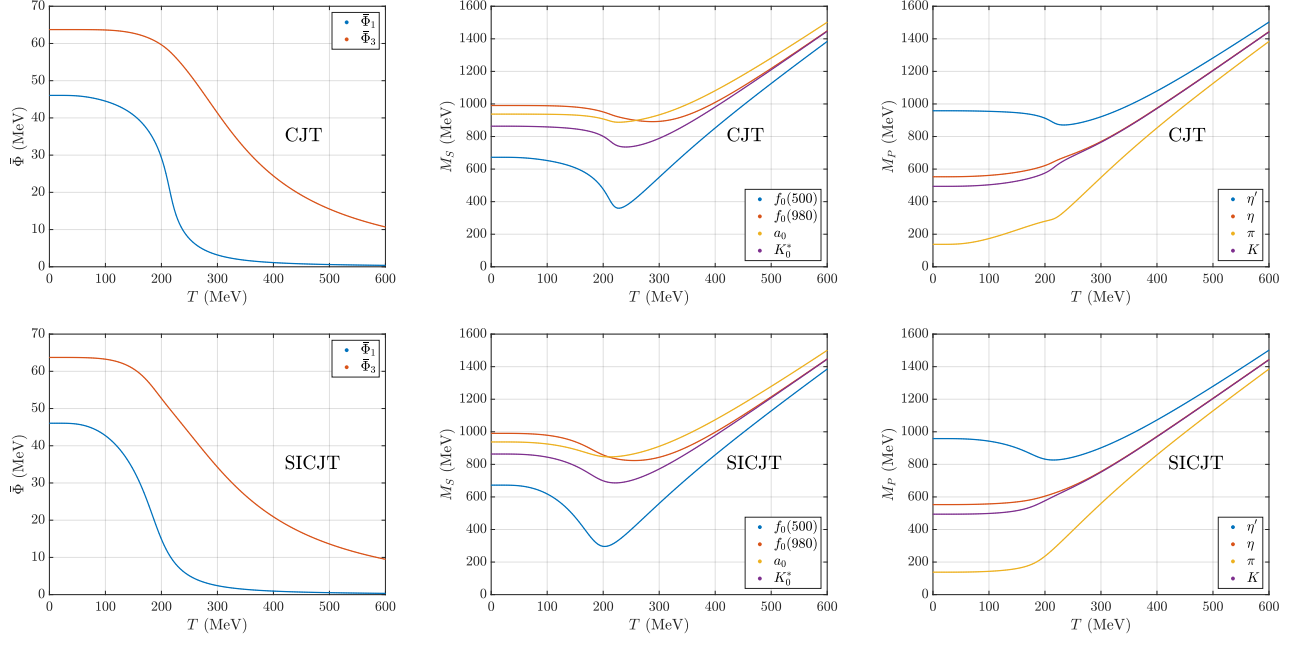


FIG. 3. Plots of  $T$ -dependences on  $\bar{\Phi}_{1,3}$  (left panel) and masses of scalar (middle) and pseudoscalar mesons (right), at the physical point, in the cases of the conventional CJT (upper panels) and SICJT (lower panels) formalisms applied to the present LSM with the parameter set I in Sec. IV B 1.

#### D. Chiral phase transition in chiral limit

We also explore the chiral phase transitions in the chiral limit at  $(m_l, m_s) = (0, 0)$ . See Fig. 4, where the plots have been created by taking the parameter set I in Sec. IV B 1, but with  $m_l = m_s = 0$ . We find the following characteristics for the phase transition in the chiral limit <sup>1</sup>:

- The chiral phase transition is first order, which takes place at the critical temperature  $T \sim 25$  MeV, in the case of the SICJT formalism (see the bottom-left panel of Fig. 4). This  $T_c$  is much smaller than the one measured based on the conventional CJT formalism, which yields  $T_c \sim 97$  MeV (see the top-left panel). This reduction can be understood by the proper reflection of the NG theorem in the chiral limit even at finite  $T$ : thermal and quantum loop corrections arising from lighter mesons tend to generate a more efficient Debye mass as  $T$  gets higher, such that the criticality is seen at lower temperatures. The presence of the first-order phase transition in both two formalisms is essentially due to the non-restoration of the  $U(1)$  axial anomaly, which is currently encoded in the KMT determinant (the  $B$  term in Eq.(5)) providing a negatively large cubic potential along the chiral-order parameter direction  $\bar{\Phi}_1$  (See also the parameter set I and II in Secs. IV B 1 and IV B 2).
- The masses of the pion  $M_\pi$  and the kaon  $M_K$  are fixed to vanish in the SICJT formalism until the exact chiral restoration (see the top-right panel of Fig. 4), while they start to develop in the CJT case at finite  $T$ , even before the chiral restoration happens (see the bottom-right panel). The former feature is closely related to the realization of the proper threshold property and the NG theorem, which is violated in the CJT formalism. More remarkably, at  $T = T_c$  in the chiral limit for the SICJT formalism, the  $f_0(500)$  mass goes to zero, reflecting the chiral partner of the massless pion.

#### E. Columbia plots

In Fig. 5, we make the Columbia plots based on the SICJT formalism (bottom panels) in comparison with the conventional CJT case (top panels). The parameter sets I and II in Secs. IV B 1 and IV B 2 have been reflected,

<sup>1</sup> In evaluating the chiral phase transition, we have omitted the solutions pointing to the local maximum, since the tachyonic modes show up (in the case of the SICJT), which brings in the numerical complexity.

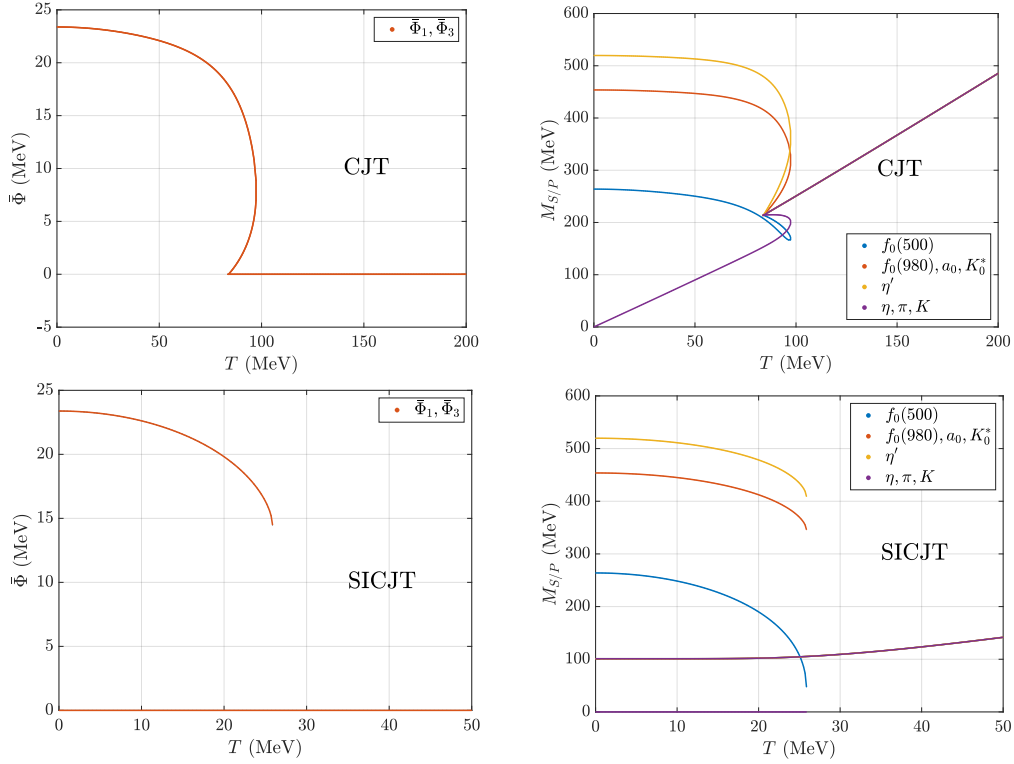


FIG. 4. The same as Fig. 3, for the chiral limit case, with the plots on the scalar and pseudoscalar meson masses combined into a single one, which has presently been summarized in the right panel.

respectively, in the left and right panels <sup>2</sup>

In the literature [33, 35], the Columbia plot has already been discussed based on a three-flavor LSM, which is similar to the present model except for the  $k$ -term (Eq.(8)), where the input observables to fix the model parameters are somewhat, but not substantially different from those used in Secs. IV B 1 and IV B 2. Currently, in the top panels of Fig. 5, we have reproduced the resulting phase structure fully consistent with the one observed in the reference, including the overall characteristics: the first-order regime is present, and two tricritical points emerge at around  $m_s = \mathcal{O}(0.1m_s^{\text{phys.}})$  and  $\gtrsim \mathcal{O}(m_s^{\text{phys.}})$  for lighter  $f_0(500)$ , while those two points get merged to be gone as  $m_{f_0(500)}$  is heavier and heavier, still keeping the presence of the first-order regime.

We find that the SICJT formalism *refines* those *artificial* and gives the *symmetry-improved* Columbia plot (bottom panels in Fig. 5): no significant  $m_{f_0(500)}$  dependence is seen, and the first-order regime as well as the single tricritical point are stably present. This can be understood by the proper realization of the low-energy theorem at finite  $T$ , which protects the pion to be light enough and safely suppresses the other heavier meson contributions in the thermal bath, including those from  $f_0(500)$ , all the way up to the chiral criticality ( $T \lesssim T_{(p)c}$ ).

We also still see from Fig 5 that in the SICJT case, the first-order regime gets shrunk when  $m_{f_0(500)}$  gets larger. This is simply due to the generation of more stringent convex negative curvature (by the negative  $\mu^2$  term in Eq.(4) with the sign choices given in Secs. IV B 1 and IV B 2). On more physics grounds, the generation of heavier  $f_0(500)$  tends to require dynamical chiral symmetry breaking essentially triggered by the negative  $\mu^2$  term, while the lighter case favors the  $U(1)$  axial anomaly to do the job.

When taking a particular look at the three-flavor symmetric limit where  $m_l = m_s$ , we find the critical quark mass on the second-order boundary (red curves in Fig. 5) to be  $m_l^c = m_s^c = 0.0939 m_l^{\text{phys.}}$ , (e.g., for the parameter set I case, in Sec. IV B 1, with  $m[f_0(500)] = 672.4$  MeV (bottom-left panel)). This quark mass value is translated into the critical pion mass at the vacuum as  $m_\pi^c = 52.4$  MeV. The criticality is observed at  $T_c \sim 51.7$  MeV.

Recently, based on highly improved staggered quarks on lattices with temporal extent  $N_\tau = 8$  [14] – which is an extension of the study with  $N_\tau = 6$  [31] – the three-flavor lattice QCD study has reported that no evidence of the

<sup>2</sup> The present analysis has been limited by the large size of  $m_s$  up to  $2m_s^{\text{phys.}}$ , above which a part of the  $k$ -term proportional to  $m_s$  (Eq.(8)) will cause an instability in the system, because of the artificial non-decoupling effect of the strange quark in the  $k$ -term. This issue needs to be fixed in a separate publication.

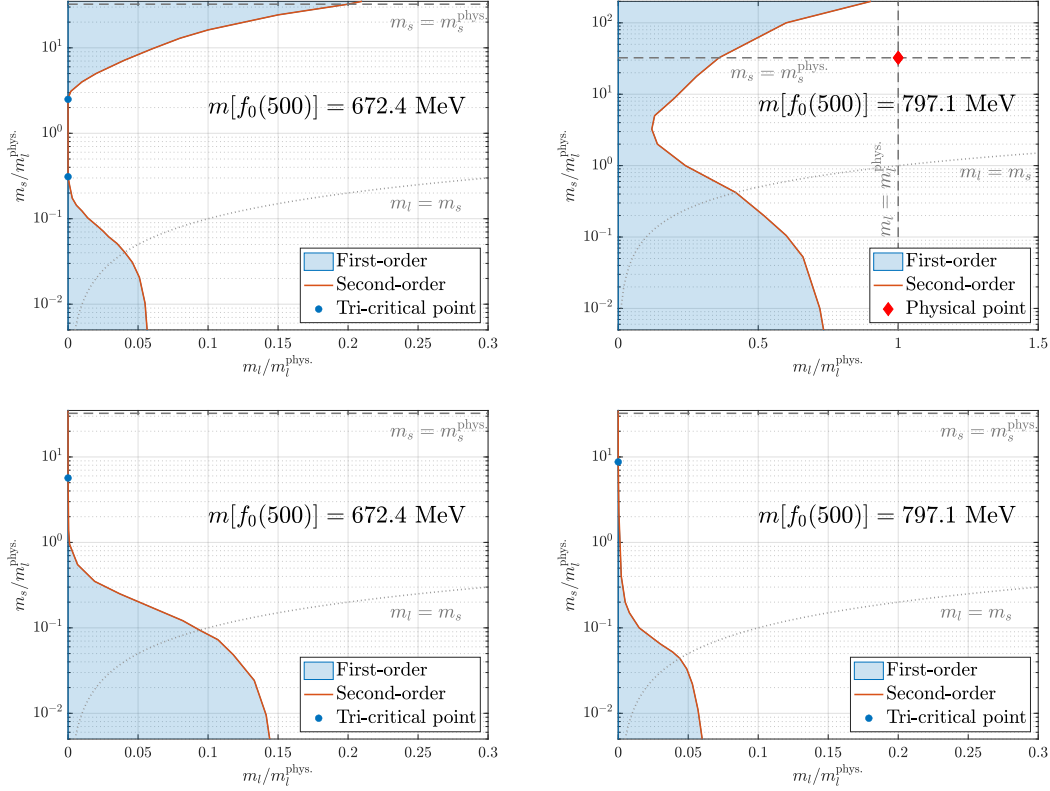


FIG. 5. The SICJT result projected onto the Columbia plots with the parameter sets I in Sec. IV B 1 (bottom-left panels) and II in Sec. IV B 2 (bottom-right panel), in comparison with the conventional CJT results (top-left and -right panels) on the same parameter setup. The orange-solid curves denote the second-order phase boundaries, and the blue-shaded areas the first-order domains. The three-flavor symmetric limit (the case with  $m_l = m_s$ ) has been drawn by the dotted curves, and the red-diamond marker corresponds to the physical point where  $(m_c, m_s) = (m_l^{\text{phys}}, m_s^{\text{phys}})$ . The  $m_l$  and  $m_s$  axes have been normalized by  $m_l^{\text{phys}}$ .

first-order signal is observed for  $m_\pi \gtrsim 80$  MeV. The critical temperature has also been estimated via the finite-size scaling analysis, to give  $T_c = 98^{+3}_{-6}$  MeV, based on the data and statistical averaging over different fit ansatz with  $m_\pi$  in a range of  $80 \text{ MeV} \lesssim m_\pi \lesssim 140$  MeV. Our estimate on  $m_\pi^c$  above is consistent with this current lattice status, where the smaller  $T_c$  for our estimate ( $\sim 51.7$  MeV) can be understood by the small  $m_\pi^c$  ( $\sim 52.4$  MeV) (or equivalently smaller quark masses) compared to values of  $m_\pi$  sampled in the data analysis on the lattice. Our critical pion mass  $\sim 50$  MeV is also compatible with the result of the previous lattice studies with highly improved staggered quarks and  $N_\tau = 6$  [31], which gives  $m_\pi^c \lesssim 50$  MeV; the nonperturbatively  $O(\alpha)$  improved Wilson-Clover quarks and  $N_\tau = 12$  [32], which gives  $m_\pi^c \lesssim 110$  MeV. The consistency can also be seen in comparison with the lattice result based on the stout action [59] with  $N_\tau = 6$ . The predicted  $m_\pi^c$  is slightly greater than what the fRG method for a quark-meson model has recently suggested:  $m_\pi^c < 25$  MeV [12].

## V. CONCLUSION

In this work, we have investigated the structure of the Columbia plot within a three-flavor LSM monitoring the underlying QCD, which exhibits the global chiral  $U(3)$  symmetry, explicitly broken by current quark masses and by the  $U(1)$  axial anomaly. We have included both leading-order anomaly terms and anomaly-induced flavor-breaking interactions, motivated by the phenomenological success of the model shown in the literature [51]. Our analysis was carried out within the CJT framework for the 2PI effective action, considering both the conventional and the symmetry-improved formulations, the latter being dubbed the SICJT [48].

A primary focus of the present work is to address the known issues in truncated 2PI approaches, particularly the violation of the NG theorem and the threshold property in the chiral broken phase. These violations get significant near the criticality of the chiral phase transition. By enforcing the WTIs for the 1PI effective action through the SICJT

formalism, we have refined the conventional CJT approach on the three-flavor LSM and analyzed the consequences for the chiral phase structure and the projection onto the Columbia plot.

Our analysis has clarified that an enhanced first-order region, which has been detected in the conventional CJT method with the standard Hartree-level approximation, is merely an artifact due to the lack of the manifest NG and low-energy theorems at finite temperature. This result suggests that a consistent incorporation of mesonic fluctuations that preserves the chiral symmetry is crucial for properly capturing the chiral phase structure, even within relatively simple truncation schemes.

Still, our current approach should potentially be applicable as a tool for studying other critical phenomena, such as the search for the critical endpoint in QCD-like theories and their LEFTs. Beyond mean-field and large- $N$  approximations, the SICJT approach would sufficiently incorporate mesonic fluctuation contributions through the self-consistent resummation of meson two-point functions by respecting the necessary symmetry constraints. Thus, our present work would provide a definite one step forward to improve the reliability to properly explore meson mass spectra near the criticality.

The symmetry-improved 2PI formalism would also offer a useful framework for exploring the QCD phase diagram in terms of LEFTs, particularly for applications at some criticality where the proper treatment of soft modes and collective excitations is essential. Other possible and simple-minded outlooks may also be involved: extending the current framework by including vector and axialvector mesons; incorporation of the coupling to Polyakov loops; finite chemical potential; the convolution with other nonperturbative methods such as the fRG; the studies of the electroweak phase transition and/or dark chiral phase transitions including physics beyond the Standard Model. In that case, in a way consistent with the (anomalous) WTIs, the SICJT formalism would help performing a proper resummation of 2PI diagram series, improving the radius of convergence like the conventional daisy resummation, and the validity of the conventional perturbative formulations.

## ACKNOWLEDGMENTS

We thank Zheng-Ze Li for fruitful discussions and contributions in the early stage of the present work. This work was supported in part by the National Science Foundation of China (NSFC) under Grant No.11747308, 11975108, 12047569, and the Seeds Funding of Jilin University (S.M.). The work by M.K. is supported by RFIS-NSFC under Grant No. W2433019. The work of A.T. was partially supported by JSPS KAKENHI Grant Numbers 20K14479, 22K03539, 22H05112, and 22H05111, and MEXT as “Program for Promoting Researches on the Supercomputer Fugaku” (Simulation for basic science: approaching the new quantum era; Grant Number JPMXP1020230411, and Search for physics beyond the standard model using large-scale lattice QCD simulation and development of AI technology toward next-generation lattice QCD; Grant Number JPMXP1020230409).

## Appendix A: The three-flavor LSM at tree-level

In this appendix, we summarize the tree-level formulae in the three-flavor LSM employed in the present paper.

### 1. The vacuum constraint by the stationary condition

At tree-level, the potential (3) along the vacuum direction specialised only by the  $(\bar{\Phi}_1, \bar{\Phi}_3)$ -background fields reads

$$V(\bar{\Phi}) = \mu^2 \left( 2\bar{\Phi}_1^2 + \bar{\Phi}_3^2 \right) + \lambda_1 \left( 2\bar{\Phi}_1^4 + \bar{\Phi}_3^4 \right) + \lambda_2 \left( 2\bar{\Phi}_1^2 + \bar{\Phi}_3^2 \right)^2 - 2B\bar{\Phi}_1^2\bar{\Phi}_3 - 2 \left( 2cm_l\bar{\Phi}_1 + cm_s\bar{\Phi}_3 \right) - 4k \left( cm_s\bar{\Phi}_1^2 + 2cm_l\bar{\Phi}_1\bar{\Phi}_3 \right). \quad (\text{A1})$$

The slopes of the classical action  $S_{\text{LSM}} = \int d^4V(\bar{\Phi})$  are then given as

$$\begin{aligned} \left. \frac{\delta S_{\text{LSM}}}{\delta \bar{\Phi}_1} \right|_{\Phi=\bar{\Phi}} &= 4 \left( \mu^2\bar{\Phi}_1 + 2\lambda_1\bar{\Phi}_1^3 + 4\lambda_2\bar{\Phi}_1^3 + 2\lambda_2\bar{\Phi}_1\bar{\Phi}_3^2 - B\bar{\Phi}_1\bar{\Phi}_3 - cm_l - 2kcm_l\bar{\Phi}_3 - 2kcm_s\bar{\Phi}_1 \right), \\ \left. \frac{\delta S_{\text{LSM}}}{\delta \bar{\Phi}_3} \right|_{\Phi=\bar{\Phi}} &= 2 \left( \mu^2\bar{\Phi}_3 + 2\lambda_1\bar{\Phi}_3^3 + 4\lambda_2\bar{\Phi}_1^2\bar{\Phi}_3 - B\bar{\Phi}_1^2 - cm_s - 4kcm_l\bar{\Phi}_1 \right). \end{aligned} \quad (\text{A2})$$

Alternatively, using Eq.(11), the tree-level potential  $V(\bar{\Phi})$  in terms of the  $(\bar{\sigma}_0, \bar{\sigma}_8)$ -background fields reads

$$\begin{aligned} V(\bar{\sigma}) = & \frac{1}{2}\mu^2(\bar{\sigma}_0^2 + \bar{\sigma}_8^2) + \lambda_1 \left[ \frac{1}{12}\bar{\sigma}_0^4 + \frac{1}{2}\bar{\sigma}_0^2\bar{\sigma}_8^2 - \frac{1}{3\sqrt{2}}\bar{\sigma}_0\bar{\sigma}_8^3 + \frac{1}{8}\bar{\sigma}_8^4 \right] + \frac{\lambda_2}{4}(\bar{\sigma}_0^2 + \bar{\sigma}_8^2)^2 \\ & - B \left[ \frac{1}{3\sqrt{6}}\bar{\sigma}_0^3 - \frac{1}{2\sqrt{6}}\bar{\sigma}_0\bar{\sigma}_8^2 - \frac{1}{6\sqrt{3}}\bar{\sigma}_8^3 \right] - \sqrt{\frac{2}{3}}(2cm_l + cm_s)\bar{\sigma}_0 - \frac{2}{\sqrt{3}}(cm_l - cm_s)\bar{\sigma}_8 \\ & - k \left[ \frac{cm_l}{3}(4\bar{\sigma}_0^2 - 2\sqrt{2}\bar{\sigma}_0\bar{\sigma}_8 - 4\bar{\sigma}_8^2) + \frac{cm_s}{3}(2\bar{\sigma}_0^2 + 2\sqrt{2}\bar{\sigma}_0\bar{\sigma}_8 + \bar{\sigma}_8^2) \right]. \end{aligned} \quad (A3)$$

The corresponding slopes of the classical action are then given as

$$\begin{aligned} \left. \frac{\delta S_{\text{LSM}}}{\delta \sigma_0} \right|_{\sigma_a = \bar{\sigma}_a} &= \mu^2 \bar{\sigma}_0 + \lambda_1 \left[ \frac{1}{3}\bar{\sigma}_0^3 + \bar{\sigma}_0\bar{\sigma}_8^2 - \frac{1}{3\sqrt{2}}\bar{\sigma}_8^3 \right] + \lambda_2(\bar{\sigma}_0^2 + \bar{\sigma}_8^2)\bar{\sigma}_0 - B \left[ \frac{1}{\sqrt{6}}\bar{\sigma}_0^2 - \frac{1}{2\sqrt{6}}\bar{\sigma}_8^2 \right] \\ &\quad - \sqrt{\frac{2}{3}}(2cm_l + cm_s) - k \left[ \frac{cm_l}{3}(8\bar{\sigma}_0 - 2\sqrt{2}\bar{\sigma}_8) + \frac{cm_s}{3}(4\bar{\sigma}_0 + 2\sqrt{2}\bar{\sigma}_8) \right], \\ \left. \frac{\delta S_{\text{LSM}}}{\delta \sigma_8} \right|_{\sigma_a = \bar{\sigma}_a} &= \mu^2 \bar{\sigma}_8 + \lambda_1 \left[ \bar{\sigma}_0^2\bar{\sigma}_8 - \frac{1}{\sqrt{2}}\bar{\sigma}_0\bar{\sigma}_8^2 + \frac{1}{2}\bar{\sigma}_8^3 \right] + \lambda_2(\bar{\sigma}_0^2 + \bar{\sigma}_8^2)\bar{\sigma}_8 + B \left[ \frac{1}{\sqrt{6}}\bar{\sigma}_0\bar{\sigma}_8 + \frac{1}{2\sqrt{3}}\bar{\sigma}_8^2 \right] \\ &\quad - \frac{2}{\sqrt{3}}(cm_l - cm_s) - k \left[ \frac{cm_l}{3}(-2\sqrt{2}\bar{\sigma}_0 - 8\bar{\sigma}_8) + \frac{cm_s}{3}(2\sqrt{2}\bar{\sigma}_0 + 2\bar{\sigma}_8) \right]. \end{aligned} \quad (A4)$$

Note that those two sets of slopes in Eqs.(A2) and (A4) are related to each other through the linear transformation arising from the chain rule as

$$\begin{pmatrix} \frac{\delta S_{\text{LSM}}}{\delta \Phi_1} \\ \frac{\delta S_{\text{LSM}}}{\delta \Phi_3} \end{pmatrix} = \begin{pmatrix} 2\sqrt{\frac{2}{3}} & \frac{2}{\sqrt{3}} \\ \sqrt{\frac{2}{3}} & -\frac{2}{\sqrt{3}} \end{pmatrix} \begin{pmatrix} \frac{\delta S_{\text{LSM}}}{\delta \sigma_0} \\ \frac{\delta S_{\text{LSM}}}{\delta \sigma_8} \end{pmatrix}. \quad (A5)$$

At the classical level, the equilibrium criteria, or the stationary conditions, read

$$\left. \frac{\delta S_{\text{LSM}}}{\delta \Phi_1} \right|_{\Phi = \bar{\Phi}} = 0, \quad \left. \frac{\delta S_{\text{LSM}}}{\delta \Phi_3} \right|_{\Phi = \bar{\Phi}} = 0. \quad (A6)$$

which is equivalent to

$$\left. \frac{\delta S_{\text{LSM}}}{\delta \sigma_0} \right|_{\sigma_a = \bar{\sigma}_a} = 0, \quad \left. \frac{\delta S_{\text{LSM}}}{\delta \sigma_8} \right|_{\sigma_a = \bar{\sigma}_a} = 0 \quad (A7)$$

through Eq. (A5).

If we adopt the  $SU(3)_V$  flavor symmetry, i.e.,  $m_l = m_s \equiv m$ , we find that the slope of the  $\sigma_8$ -direction in Eq.(A5) becomes

$$\left. \frac{\delta S_{\text{LSM}}}{\delta \sigma_8} \right|_{\sigma_a = \bar{\sigma}_a} = \bar{\sigma}_8 \left\{ \mu^2 + \lambda_1 \left[ \bar{\sigma}_0^2 - \frac{1}{\sqrt{2}}\bar{\sigma}_0\bar{\sigma}_8 + \frac{1}{2}\bar{\sigma}_8^2 \right] + \lambda_2(\bar{\sigma}_0^2 + \bar{\sigma}_8^2) + B \left[ \frac{1}{\sqrt{6}}\bar{\sigma}_0 + \frac{1}{2\sqrt{3}}\bar{\sigma}_8 \right] + 2kcm \right\}. \quad (A8)$$

The stationary condition along this  $\sigma_8$  direction thus includes the trivial solution  $\bar{\sigma}_8 = 0$ , i.e.,  $\bar{\Phi}_1 = \bar{\Phi}_3$ , which precisely reflects the  $SU(3)_V$  symmetry. This flavor symmetric solution can also be realized when we re-arrange Eq. (A2) as follows:

$$\begin{aligned} \frac{1}{4} \frac{\delta S_{\text{LSM}}}{\delta \Phi_1} \Big|_{\Phi = \bar{\Phi}} - \frac{1}{2} \frac{\delta S_{\text{LSM}}}{\delta \Phi_3} \Big|_{\Phi = \bar{\Phi}} &= (\bar{\Phi}_1 - \bar{\Phi}_3) \left[ \mu^2 + 2\lambda_1(\bar{\Phi}_1^2 + \bar{\Phi}_1\bar{\Phi}_3 + \bar{\Phi}_3^2) \right. \\ &\quad \left. + \lambda_2(4\bar{\Phi}_1^2 + 2\bar{\Phi}_3^2) + B\bar{\Phi}_1 + 2kcm_l \right] - (cm_l - cm_s)(1 - 2k\bar{\Phi}_1). \end{aligned} \quad (A9)$$

We thus find the trivial solution  $\bar{\Phi}_1 - \bar{\Phi}_3 = 0$  when  $m_l = m_s$ .

## 2. Curvature masses

The LSM field  $\Phi$  includes the scalar and pseudoscalar meson fields as  $\Phi = \phi_a T^a = (\sigma_a + i\pi_a)T^a$  for  $a = 0, \dots, 8$ . The Hessian matrix with respect to those meson fields is found by taking the second functional derivative for  $S_{\text{LSM}} = \int_x \mathcal{L}_{\text{LSM}}$  with  $\mathcal{L}_{\text{LSM}}$  in Eq.(2). It is in four-dimensional momentum space given as

$$\begin{aligned} \left[ \bar{S}^{-1}(k, k'; \bar{\sigma}) \right]^{ab} &= \frac{\delta^2 S_{\text{LSM}}}{\delta \sigma_a(-k') \delta \sigma_b(k)} = (2\pi)^4 \delta^{(4)}(k - k') \left( k^2 \delta^{ab} + \left[ m_S^2(\bar{\sigma}) \right]^{ab} \right) \\ &\equiv (2\pi)^4 \delta^{(4)}(k - k') \left[ \bar{S}^{-1}(k; \bar{\sigma}) \right]^{ab}, \\ \left[ \bar{P}^{-1}(k, k'; \bar{\sigma}) \right]^{ab} &= \frac{\delta^2 S_{\text{LSM}}}{\delta \pi_a(-k') \delta \pi_b(k)} = (2\pi)^4 \delta^{(4)}(k - k') \left( k^2 \delta^{ab} + \left[ m_P^2(\bar{\sigma}) \right]^{ab} \right) \\ &\equiv (2\pi)^4 \delta^{(4)}(k - k') \left[ \bar{P}^{-1}(k; \bar{\sigma}) \right]^{ab}, \end{aligned} \quad (\text{A10})$$

where we have defined the tree-level curvature masses as

$$\left[ m_S^2(\bar{\sigma}) \right]^{ab} = \frac{\partial^2 V_{\text{LSM}}}{\partial \sigma_a \partial \sigma_b} \bigg|_{\sigma_a = \bar{\sigma}_a}, \quad \left[ m_P^2(\bar{\sigma}) \right]^{ab} = \frac{\partial^2 V_{\text{LSM}}}{\partial \pi_a \partial \pi_b} \bigg|_{\sigma_a = \bar{\sigma}_a}. \quad (\text{A11})$$

Notice that the mixing matrix elements such as  $\frac{\delta^2 S_{\text{LSM}}}{\delta \pi_a(-k') \delta \sigma_b(k)}$  vanish because of the parity invariance. From Eq.(A11) the matrix elements for the square of the nonet scalar meson masses read

$$\begin{aligned} \left[ m_S^2(\bar{\sigma}) \right]^{00} &= \mu^2 + \lambda_1 (\bar{\sigma}_0^2 + \bar{\sigma}_8^2) + \lambda_2 (3\bar{\sigma}_0^2 + \bar{\sigma}_8^2) - B \sqrt{\frac{2}{3}} \bar{\sigma}_0 - \frac{4}{3} k (2cm_l + cm_s), \\ \left[ m_S^2(\bar{\sigma}) \right]^{88} &= \mu^2 + \lambda_1 \left[ \bar{\sigma}_0^2 - \sqrt{2} \bar{\sigma}_0 \bar{\sigma}_8 + \frac{3}{2} \bar{\sigma}_8^2 \right] + \lambda_2 (\bar{\sigma}_0^2 + 3\bar{\sigma}_8^2) + \frac{B}{\sqrt{3}} \left[ \frac{1}{\sqrt{2}} \bar{\sigma}_0 + \bar{\sigma}_8 \right] + \frac{2}{3} k (4cm_l - cm_s), \\ \left[ m_S^2(\bar{\sigma}) \right]^{08} &= \left[ m_S^2(\bar{\sigma}) \right]^{80} = \lambda_1 \left[ 2\bar{\sigma}_0 \bar{\sigma}_8 - \frac{1}{\sqrt{2}} \bar{\sigma}_8^2 \right] + 2\lambda_2 \bar{\sigma}_0 \bar{\sigma}_8 + \frac{B}{\sqrt{6}} \bar{\sigma}_8 + \frac{2\sqrt{2}}{3} k (cm_l - cm_s), \\ \left[ m_S^2(\bar{\sigma}) \right]^{11} &= \left[ m_S^2(\bar{\sigma}) \right]^{22} = \left[ m_S^2(\bar{\sigma}) \right]^{33} \\ &= \mu^2 + \lambda_1 \left[ \bar{\sigma}_0^2 + \sqrt{2} \bar{\sigma}_0 \bar{\sigma}_8 + \frac{1}{2} \bar{\sigma}_8^2 \right] + \lambda_2 (\bar{\sigma}_0^2 + \bar{\sigma}_8^2) + \frac{B}{\sqrt{3}} \left[ \frac{1}{\sqrt{2}} \bar{\sigma}_0 - \bar{\sigma}_8 \right] + 2kcm_s, \\ \left[ m_S^2(\bar{\sigma}) \right]^{44} &= \left[ m_S^2(\bar{\sigma}) \right]^{55} = \left[ m_S^2(\bar{\sigma}) \right]^{66} = \left[ m_S^2(\bar{\sigma}) \right]^{77} \\ &= \mu^2 + \lambda_1 \left[ \bar{\sigma}_0^2 - \frac{1}{\sqrt{2}} \bar{\sigma}_0 \bar{\sigma}_8 + \frac{1}{2} \bar{\sigma}_8^2 \right] + \lambda_2 (\bar{\sigma}_0^2 + \bar{\sigma}_8^2) + \frac{B}{\sqrt{3}} \left[ \frac{1}{\sqrt{2}} \bar{\sigma}_0 + \frac{1}{2} \bar{\sigma}_8 \right] + 2kcm_l, \\ (\text{Others}) &= 0. \end{aligned} \quad (\text{A12})$$

The matrix elements  $\left[ m_S^2(\bar{\sigma}) \right]^{11}$  and  $\left[ m_S^2(\bar{\sigma}) \right]^{44}$  are identified as the square of the  $a_0(980)$  mass,  $m_{a_0}^2$ , and the  $\kappa(700) = K_0^*(700)$  mass,  $m_\kappa^2$ , respectively. The mixed  $(\sigma_0, \sigma_8)$  sector can be diagonalized through an orthogonal transformation

$$\begin{aligned} \tilde{\sigma}_i &= (O_S^{-1})_i^a \sigma_a, \\ \left[ \tilde{m}_S^2(\bar{\sigma}) \right]_{(i)}^{ij} &= (O_S^{-1})_a^i \left[ m_S^2(\bar{\sigma}) \right]^{ab} (O_S)_b^j, \end{aligned} \quad (\text{A13})$$

where  $\left[ \tilde{m}_S^2(\bar{\sigma}) \right]_{(i)}$  denotes the diagonalized scalar mass matrix, and the orthogonal transformation matrix  $O_S$  is given as

$$O_S = \begin{pmatrix} \cos \theta_S^0 & -\sin \theta_S^0 \\ \sin \theta_S^0 & \cos \theta_S^0 \end{pmatrix}, \quad (\text{A14})$$



with the mixing angle,

$$\theta_S^0 = \frac{1}{2} \arctan \left[ \frac{2[m_S^2(\bar{\sigma})]^{08}}{[m_S^2(\bar{\sigma})]^{00} - [m_S^2(\bar{\sigma})]^{88}} \right]. \quad (\text{A15})$$

Note that in the three-flavor symmetric limit where  $\bar{\sigma}_8 = 0$  and  $m_1 = m_s = m$ , the off diagonal element  $[m_S^2(\bar{\sigma})]^{08}$  vanishes. The  $f_0(500)$  and the  $f_0(980)$  masses are identified through the lowest and highest eigenvalues, respectively, as

$$\begin{aligned} m^2[f_0(500)] &= [\tilde{m}_S^2(\bar{\sigma})]_{(0)} = [m_S^2(\bar{\sigma})]^{00} \cos^2 \theta_S^0 + [m_S^2(\bar{\sigma})]^{88} \sin^2 \theta_S^0 + 2[m_S^2(\bar{\sigma})]^{08} \cos \theta_S^0 \sin \theta_S^0, \\ m^2[f_0(980)] &= [\tilde{m}_S^2(\bar{\sigma})]_{(8)} = [m_S^2(\bar{\sigma})]^{00} \sin^2 \theta_S^0 + [m_S^2(\bar{\sigma})]^{88} \cos^2 \theta_S^0 - 2[m_S^2(\bar{\sigma})]^{08} \cos \theta_S^0 \sin \theta_S^0. \end{aligned} \quad (\text{A16})$$

Similarly, from Eq.(A11), the matrix elements for the square of the nonet pseudoscalar meson masses are read off as

$$\begin{aligned} [m_P^2(\bar{\sigma})]^{00} &= \mu^2 + \frac{\lambda_1}{3} (\bar{\sigma}_0^2 + \bar{\sigma}_8^2) + \lambda_2 (\bar{\sigma}_0^2 + \bar{\sigma}_8^2) + B \sqrt{\frac{2}{3}} \bar{\sigma}_0 + \frac{4}{3} k (2cm_l + cm_s), \\ [m_P^2(\bar{\sigma})]^{88} &= \mu^2 + \lambda_1 \left[ \frac{1}{3} \bar{\sigma}_0^2 - \frac{\sqrt{2}}{3} \bar{\sigma}_0 \bar{\sigma}_8 + \frac{1}{2} \bar{\sigma}_8^2 \right] + \lambda_2 (\bar{\sigma}_0^2 + \bar{\sigma}_8^2) - \frac{B}{\sqrt{3}} \left[ \frac{1}{\sqrt{2}} \bar{\sigma}_0 + \bar{\sigma}_8 \right] - \frac{2}{3} k (4cm_l - cm_s), \\ [m_P^2(\bar{\sigma})]^{08} &= [m_P^2(\bar{\sigma})]^{80} = \frac{\lambda_1}{3} \left[ 2\bar{\sigma}_0 \bar{\sigma}_8 - \frac{1}{\sqrt{2}} \bar{\sigma}_8^2 \right] - \frac{B}{\sqrt{6}} \bar{\sigma}_8 - \frac{2\sqrt{2}}{3} k (cm_l - cm_s), \\ [m_P^2(\bar{\sigma})]^{11} &= [m_P^2(\bar{\sigma})]^{22} = [m_P^2(\bar{\sigma})]^{33} \\ &= \mu^2 + \frac{\lambda_1}{3} \left[ \bar{\sigma}_0^2 + \sqrt{2} \bar{\sigma}_0 \bar{\sigma}_8 + \frac{1}{2} \bar{\sigma}_8^2 \right] + \lambda_2 (\bar{\sigma}_0^2 + \bar{\sigma}_8^2) - \frac{B}{\sqrt{3}} \left[ \frac{1}{\sqrt{2}} \bar{\sigma}_0 - \bar{\sigma}_8 \right] - 2kcm_s, \\ [m_P^2(\bar{\sigma})]^{44} &= [m_P^2(\bar{\sigma})]^{55} = [m_P^2(\bar{\sigma})]^{66} = [m_P^2(\bar{\sigma})]^{77} \\ &= \mu^2 + \frac{\lambda_1}{3} \left[ \bar{\sigma}_0^2 - \frac{1}{\sqrt{2}} \bar{\sigma}_0 \bar{\sigma}_8 + \frac{7}{2} \bar{\sigma}_8^2 \right] + \lambda_2 (\bar{\sigma}_0^2 + \bar{\sigma}_8^2) - \frac{B}{\sqrt{3}} \left[ \frac{1}{\sqrt{2}} \bar{\sigma}_0 + \frac{1}{2} \bar{\sigma}_8 \right] - 2kcm_l, \\ (\text{Others}) &= 0. \end{aligned} \quad (\text{A17})$$

The matrix elements  $[m_P^2(\bar{\sigma})]^{11}$  and  $[m_P^2(\bar{\sigma})]^{44}$  are identified as the squares of the pion mass,  $m_\pi^2$ , and the kaon mass  $m_K^2$ , respectively. The mixed  $(\pi_0, \pi_8)$  sector can be diagonalized through an orthogonal transformation, similarly to the  $(\sigma_0, \sigma_8)$  sector in Eq.(A13) as

$$\begin{aligned} \tilde{\pi}_i &= (O_P^{-1})^a_i \pi_a, \\ [\tilde{m}_P^2(\bar{\sigma})]_{(i)} \delta^{ij} &= (O_P^{-1})^i_a [m_P^2(\bar{\sigma})]^{ab} (O_P)_b^j, \end{aligned} \quad (\text{A18})$$

where  $[\tilde{m}_P^2(\bar{\sigma})]_{(i)}$  denotes the diagonalized pseudoscalar meson mass matrix, and the transformation matrix  $O_P$  reads

$$O_S = \begin{pmatrix} \cos \theta_P^0 & -\sin \theta_P^0 \\ \sin \theta_P^0 & \cos \theta_P^0 \end{pmatrix}. \quad (\text{A19})$$

with the mixing angle,

$$\theta_P^0 = \frac{1}{2} \arctan \left[ \frac{2[m_P^2(\bar{\sigma})]^{08}}{[m_P^2(\bar{\sigma})]^{00} - [m_P^2(\bar{\sigma})]^{88}} \right]. \quad (\text{A20})$$

The off diagonal element  $\left[m_P^2(\bar{\sigma})\right]^{08}$  vanishes in the three-flavor symmetric limit where  $\bar{\sigma}_8 = 0$ . Then, the  $\eta'$  and the  $\eta$  masses are identified through the eigenvalues

$$\begin{aligned} m_{\eta'}^2 &= \left[\tilde{m}_P^2(\bar{\sigma})\right]_{(0)} = \left[m_P^2(\bar{\sigma})\right]^{00} \cos^2 \theta_P^0 + \left[m_P^2(\bar{\sigma})\right]^{88} \sin^2 \theta_P^0 + 2 \left[m_P^2(\bar{\sigma})\right]^{08} \cos \theta_P^0 \sin \theta_P^0, \\ m_{\eta}^2 &= \left[\tilde{m}_P^2(\bar{\sigma})\right]_{(8)} = \left[m_P^2(\bar{\sigma})\right]^{00} \sin^2 \theta_P^0 + \left[m_P^2(\bar{\sigma})\right]^{88} \cos^2 \theta_P^0 - 2 \left[m_P^2(\bar{\sigma})\right]^{08} \cos \theta_P^0 \sin \theta_P^0. \end{aligned} \quad (\text{A21})$$

## Appendix B: CJT formalism at finite temperature

In this appendix, we summarize the formulations in the conventional CJT formalism applied to the present LSM at finite temperature.

### 1. CJT formalism and Hartree approximation

We begin by recasting the CJT effective potential given by Eq. (14), i.e.,

$$\begin{aligned} V_{\text{CJT}}[\sigma, S, P] &= V(\sigma) + \frac{1}{2} \int_k \text{tr} \left[ \log S^{-1}(k) + \log P^{-1}(k) \right] \\ &\quad + \frac{1}{2} \int_k \text{tr} \left[ \bar{S}^{-1}(k; \sigma) S(k) + \bar{P}^{-1}(k; \sigma) P(k) - 2 \right] + V_2[\sigma, S, P]. \end{aligned} \quad (\text{B1})$$

Here, the shorthand notation of the momentum integral is defined as

$$\int_k f(k) = T \sum_{n=-\infty}^{\infty} \int \frac{d^3 \mathbf{k}}{(2\pi)^3} f(\omega_n, \mathbf{k}), \quad (\text{B2})$$

with  $\omega_n = 2n\pi T$  being the bosonic Matsubara frequency. The tree-level mesonic propagators  $\bar{S}(k; \bar{\sigma})$  and  $\bar{P}(k; \bar{\sigma})$  are defined as

$$\begin{aligned} \left[\bar{S}^{-1}(k; \sigma)\right]^{ab} &= k^2 \delta^{ab} + \left[m_S^2(\sigma)\right]^{ab}, \\ \left[\bar{P}^{-1}(k; \sigma)\right]^{ab} &= k^2 \delta^{ab} + \left[m_P^2(\sigma)\right]^{ab}, \end{aligned} \quad (\text{B3})$$

where  $m_S^2(\bar{\sigma})$  and  $m_P^2(\bar{\sigma})$  are the mesonic curvature masses which are read off from Eqs. (A12) and (A17).

The VEV of  $\sigma$  and the propagators  $S$  and  $\bar{P}$  are determined the stationary conditions and the gap equations

$$\begin{aligned} \left. \frac{\partial V_{\text{CJT}}[\sigma, S, P]}{\partial \sigma_a} \right|_{\sigma=\bar{\sigma}, S=\mathcal{S}, P=\mathcal{P}} &= 0, \\ \left. \frac{\delta V_{\text{CJT}}[\sigma, S, P]}{\delta S_{ab}} \right|_{\sigma=\bar{\sigma}, S=\mathcal{S}, P=\mathcal{P}} &= 0, \\ \left. \frac{\delta V_{\text{CJT}}[\sigma, S, P]}{\delta P_{ab}} \right|_{\sigma=\bar{\sigma}, S=\mathcal{S}, P=\mathcal{P}} &= 0. \end{aligned} \quad (\text{B4})$$

The latter two gap equations can be expressed as

$$\begin{aligned} \left[\mathcal{S}^{-1}(k)\right]^{ab} &= \left[\bar{S}^{-1}(k; \sigma)\right]^{ab} + \Sigma^{ab}, \\ \left[\mathcal{P}^{-1}(k)\right]^{ab} &= \left[\bar{P}^{-1}(k; \sigma)\right]^{ab} + \Pi^{ab}, \end{aligned} \quad (\text{B5})$$

where

$$\begin{aligned}\Sigma^{ab} &= 2 \frac{\delta V_2[\sigma, S, P]}{\delta S_{ba}} \bigg|_{\sigma=\bar{\sigma}, S=S, P=P}, \\ \Pi^{ab} &= 2 \frac{\delta V_2[\sigma, S, P]}{\delta P_{ba}} \bigg|_{\sigma=\bar{\sigma}, S=S, P=P},\end{aligned}\quad (\text{B6})$$

are the meson self-energies, which also depend on  $S$  and  $P$ . Notice that if we take  $V_2 = 0$ , in the gap equations in Eq.(B5), the propagators are replaced by the tree-level ones, thus the 2PI effective potential will be reduced to the 1PI effective action at one-loop level.

Since  $V_2$  includes infinite 2PI diagrams, we have to make a truncation to close the stationary condition and gap equations in Eq.(B5). In the present work, we apply the double-bubble diagram truncation, as depicted in Fig. 1, for which the truncation scheme is equivalent to the so-called Hartree approximation. The thus truncated 2PI diagrams are generated from the four-meson interactions in  $V_0$  given in Eq.(3), which reads

$$V_2[S, P] = \mathcal{F}^{abcd} \left[ \int_k S_{ab}(k) \int_q S_{cd}(q) + \int_k P_{ab}(k) \int_q P_{cd}(q) \right] + 2\mathcal{H}^{abcd} \int_k S_{ab}(k) \int_q P_{cd}(q), \quad (\text{B7})$$

where

$$\begin{aligned}\mathcal{F}^{abcd} &\equiv \frac{1}{8} \frac{\partial^4 V_0}{\partial \sigma_a \partial \sigma_b \partial \sigma_c \partial \sigma_d} \bigg|_{\Phi=0} = \frac{\lambda_1}{8} \left( d^{abn} d^{mcd} + d^{adn} d^{nbc} + d^{acn} d^{nbd} \right) + \frac{\lambda_2}{4} \left( \delta^{ab} \delta^{cd} + \delta^{ad} \delta^{bc} + \delta^{ac} \delta^{bd} \right), \\ \mathcal{H}^{abcd} &\equiv \frac{1}{8} \frac{\partial^4 V_0}{\partial \sigma_a \partial \sigma_b \partial \pi_c \partial \pi_d} \bigg|_{\Phi=0} = \frac{\lambda_1}{8} \left( d^{abn} d^{mcd} + f^{acn} f^{nbd} + f^{bcn} f^{nad} \right) + \frac{\lambda_2}{4} \delta^{ab} \delta^{cd},\end{aligned}\quad (\text{B8})$$

and the structure constants are defined as

$$d^{abc} = 2 \text{tr} \left[ \{T^a, T^b\} T^c \right], \quad f^{abc} = -2i \text{tr} \left[ [T^a, T^b] T^c \right]. \quad (\text{B9})$$

## 2. Gap equations of meson masses

Under the Hartree approximation as in Eq.(B7), the loop correction does not generate the momentum-dependent terms. As has been done in Eq. (18) of the main text, we may therefore parameterize the full-propagators as

$$\begin{aligned}\left[ \mathcal{S}^{-1}(k) \right]^{ab} &= k^2 \delta^{ab} + \left[ M_S^2 \right]^{ab}, \\ \left[ \mathcal{P}^{-1}(k) \right]^{ab} &= k^2 \delta^{ab} + \left[ M_P^2 \right]^{ab},\end{aligned}\quad (\text{B10})$$

where  $\left[ M_S \right]^{ab}$  and  $\left[ M_P \right]^{ab}$  are the full masses which include quantum and thermal corrections. Then, the gap equations in Eq.(B5) are reduced to

$$\begin{aligned}\left[ M_S^2 \right]^{ab} &= \left[ m_S^2(\bar{\sigma}) \right]^{ab} + 4\mathcal{F}^{abcd} \int_k \mathcal{S}_{cd}(k) + 4\mathcal{H}^{abcd} \int_k \mathcal{P}_{cd}(k), \\ \left[ M_P^2 \right]^{ab} &= \left[ m_P^2(\bar{\sigma}) \right]^{ab} + 4\mathcal{F}^{abcd} \int_k \mathcal{P}_{cd}(k) + 4\mathcal{H}^{abcd} \int_k \mathcal{S}_{cd}(k).\end{aligned}\quad (\text{B11})$$

At the classical level, we diagonalize the mass matrices to obtain the mass eigenstates, see Eqs. (A16) and (A21). After incorporating the quantum and thermal corrections into the meson propagators, we also introduce the following orthogonal transformations to diagonalize the full masses, in such a way that

$$\left[ \tilde{M}_{S/P}^2 \right]_{(i)} \delta^{ij} = (O'_{S/P})^i_a \left[ M_{S/P}^2 \right]^{ab} (O'_{S/P})_b^j. \quad (\text{B12})$$

The rotation angles are expressed as

$$\theta_{S/P} = \frac{1}{2} \arctan \left[ \frac{2 [M_{S/P}^2]^{08}}{[M_{S/P}^2]^{00} - [M_{S/P}^2]^{88}} \right]. \quad (\text{B13})$$

In general, the transformation matrices  $O'_{S/P}$  are different from those at the tree-level, i.e., Eqs. (A13) and (A18).

The full-propagators  $\mathcal{S}$  and  $\mathcal{P}$  can also be diagonalized simultaneously by  $O'_{S/P}$  in Eq.(B12), which goes like

$$\begin{aligned} \tilde{\mathcal{S}}_{(i)}(k) \delta_{ij} &= (O_S'^{-1})_i^a \mathcal{S}_{ab}(k) (O_S')_j^b, \\ \tilde{\mathcal{P}}_{(i)}(k) \delta_{ij} &= (O_P'^{-1})_i^a \mathcal{P}_{ab}(k) (O_P')_j^b. \end{aligned} \quad (\text{B14})$$

Then, the diagonalized meson propagators are represented fully in terms of the mass eigenvalues, i.e.,

$$\tilde{\mathcal{S}}_{(i)}^{-1}(k) = k^2 + [\tilde{M}_S^2]_{(i)}, \quad \tilde{\mathcal{P}}_{(i)}^{-1}(k) = k^2 + [\tilde{M}_P^2]_{(i)}, \quad (\text{B15})$$

where the loop corrections constructed from the meson propagators only include the form

$$\int_k \tilde{\mathcal{S}}_{(i)}(k) \quad \text{and} \quad \int_k \tilde{\mathcal{P}}_{(i)}(k). \quad (\text{B16})$$

Here, we show the expressions of the diagonalized scalar meson self-energies  $\tilde{\sigma}_{(i)}$  explicitly as

$$\begin{aligned} \tilde{\Sigma}_{(0)} &= \int_k \tilde{\mathcal{S}}_{(0)}(k) \cdot \frac{1}{16} \left[ 27\lambda_1 + 48\lambda_2 - \lambda_1 \left( 4\cos(2\theta_S) + 7\cos(4\theta_S) + 32\sqrt{2}\cos\theta_S \sin^3\theta_S \right) \right] \\ &+ \int_k \tilde{\mathcal{S}}_{(8)}(k) \cdot \frac{1}{16} \left[ 9\lambda_1 + 16\lambda_2 + \lambda_1 \left( 7\cos(4\theta_S) - 4\sqrt{2}\sin(4\theta_S) \right) \right] \\ &+ \int_k \tilde{\mathcal{S}}_{(1)}(k) \cdot \frac{3}{4} \left[ 3\lambda_1 + 4\lambda_2 + \lambda_1 \left( \cos(2\theta_S) + 2\sqrt{2}\sin(2\theta_S) \right) \right] \\ &+ \int_k \tilde{\mathcal{S}}_{(4)}(k) \cdot \left[ 3\lambda_1 + 4\lambda_2 + \lambda_1 \left( \cos(2\theta_S) - \sqrt{2}\sin(2\theta_S) \right) \right] \\ &+ \int_k \tilde{\mathcal{P}}_{(0)}(k) \cdot \frac{1}{24} \left[ 9\lambda_1 + 24\lambda_2 - \lambda_1 \cos(2\theta_P) \right. \\ &\quad \left. + \lambda_1 \sin(\theta_P) \left( -4\sqrt{2}\cos\theta_P + 4\sqrt{2}\cos(\theta_P + 2\theta_S) - 9\sin(\theta_P - 2\theta_S) + 7\sin(\theta_P + 2\theta_S) \right) \right] \\ &+ \int_k \tilde{\mathcal{P}}_{(8)}(k) \cdot \frac{1}{24} \left[ 9\lambda_1 + 24\lambda_2 + \lambda_1 \cos(2\theta_P) \right. \\ &\quad \left. + \lambda_1 \cos(\theta_P) \left( -9\cos(\theta_P - 2\theta_S) + 7\cos(\theta_P + 2\theta_S) - 8\sqrt{2}\cos(\theta_P + \theta_S) \sin\theta_S \right) \right] \\ &+ \int_k \tilde{\mathcal{P}}_{(1)}(k) \cdot \frac{1}{4} \left[ 3\lambda_1 + 12\lambda_2 + \lambda_1 \left( \cos(2\theta_S) + 2\sqrt{2}\sin(2\theta_S) \right) \right] \\ &+ \int_k \tilde{\mathcal{P}}_{(4)}(k) \cdot \frac{1}{3} \left[ 9\lambda_1 + 12\lambda_2 - \lambda_1 \left( 5\cos(2\theta_S) + \sqrt{2}\sin(2\theta_S) \right) \right], \end{aligned} \quad (\text{B17})$$

$$\begin{aligned} \tilde{\Sigma}_{(8)} &= \int_k \tilde{\mathcal{S}}_{(0)}(k) \cdot \frac{1}{16} \left[ 9\lambda_1 + 16\lambda_2 + \lambda_1 \left( 7\cos(4\theta_S) - 4\sqrt{2}\sin(4\theta_S) \right) \right] \\ &+ \int_k \tilde{\mathcal{S}}_{(8)}(k) \cdot \frac{1}{16} \left[ 27\lambda_1 + 48\lambda_2 + \lambda_1 \left( 4\cos(2\theta_S) - 7\cos(4\theta_S) + 32\sqrt{2}\cos^3\theta_S \sin\theta_S \right) \right] \\ &+ \int_k \tilde{\mathcal{S}}_{(1)}(k) \cdot \frac{3}{4} \left[ 3\lambda_1 + 4\lambda_2 - \lambda_1 \left( \cos(2\theta_S) + 2\sqrt{2}\sin(2\theta_S) \right) \right] \\ &+ \int_k \tilde{\mathcal{S}}_{(4)}(k) \cdot \left[ 3\lambda_1 + 4\lambda_2 - \lambda_1 \left( \cos(2\theta_S) - \sqrt{2}\sin(2\theta_S) \right) \right] \\ &+ \int_k \tilde{\mathcal{P}}_{(0)}(k) \cdot \frac{1}{24} \left[ 9\lambda_1 + 24\lambda_2 - \lambda_1 \cos(2\theta_P) \right] \end{aligned}$$

$$\begin{aligned}
& + 2\lambda_1 \sin(\theta_P) \left( \cos(2\theta_S) \sin \theta_P - 4 \cos \theta_S (\sqrt{2} \cos(\theta_S + \theta_P) + 4 \cos(\theta_P) \sin(\theta_S)) \right) \Big] \\
& + \int_k \tilde{\mathcal{P}}_{(8)}(k) \cdot \frac{1}{24} \left[ 9\lambda_1 + 24\lambda_2 + \lambda_1 \cos(2\theta_P) \right. \\
& \quad \left. + \lambda_1 \cos(\theta_P) \left( 9 \cos(\theta_P - 2\theta_S) - 7 \cos(\theta_P + 2\theta_S) + 8\sqrt{2} \cos \theta_S \sin(\theta_P + \theta_S) \right) \right] \\
& + \int_k \tilde{\mathcal{P}}_{(1)}(k) \cdot \frac{1}{4} \left[ 3\lambda_1 + 12\lambda_2 - \lambda_1 \left( \cos(2\theta_S) + 2\sqrt{2} \sin(2\theta_S) \right) \right] \\
& + \int_k \tilde{\mathcal{P}}_{(4)}(k) \cdot \frac{1}{3} \left[ 9\lambda_1 + 12\lambda_2 + \lambda_1 \left( 5 \cos(2\theta_S) + \sqrt{2} \sin(2\theta_S) \right) \right], \tag{B18}
\end{aligned}$$

$$\begin{aligned}
\tilde{\Sigma}_{(1)} = & \int_k \tilde{\mathcal{S}}_{(0)}(k) \cdot \frac{1}{4} \left[ 3\lambda_1 + 4\lambda_2 + \lambda_1 \left( \cos(2\theta_S) + 2\sqrt{2} \sin(2\theta_S) \right) \right] \\
& + \int_k \tilde{\mathcal{S}}_{(8)}(k) \cdot \frac{1}{4} \left[ 3\lambda_1 + 4\lambda_2 - \lambda_1 \left( \cos(2\theta_S) + 2\sqrt{2} \sin(2\theta_S) \right) \right] \\
& + \int_k \tilde{\mathcal{S}}_{(1)}(k) \cdot \frac{5}{2} \left[ \lambda_1 + 2\lambda_2 \right] \\
& + \int_k \tilde{\mathcal{S}}_{(4)}(k) \cdot 2 \left[ \lambda_1 + 2\lambda_2 \right] \\
& + \int_k \tilde{\mathcal{P}}_{(0)}(k) \cdot \frac{1}{12} \left[ 3\lambda_1 + 12\lambda_2 + \lambda_1 \left( \cos(2\theta_P) + 2\sqrt{2} \sin(2\theta_P) \right) \right] \\
& + \int_k \tilde{\mathcal{P}}_{(8)}(k) \cdot \frac{1}{12} \left[ 3\lambda_1 + 12\lambda_2 - \lambda_1 \left( \cos(2\theta_P) + 2\sqrt{2} \sin(2\theta_P) \right) \right] \\
& + \int_k \tilde{\mathcal{P}}_{(1)}(k) \cdot \frac{1}{2} \left[ 7\lambda_1 + 6\lambda_2 \right] \\
& + \int_k \tilde{\mathcal{P}}_{(4)}(k) \cdot 2 \left[ \lambda_1 + 2\lambda_2 \right], \tag{B19}
\end{aligned}$$

$$\begin{aligned}
\tilde{\Sigma}_{(4)} = & \int_k \tilde{\mathcal{S}}_{(0)}(k) \cdot \frac{1}{4} \left[ 3\lambda_1 + 4\lambda_2 + \lambda_1 \left( \cos(2\theta_S) - \sqrt{2} \sin(2\theta_S) \right) \right] \\
& + \int_k \tilde{\mathcal{S}}_{(8)}(k) \cdot \frac{1}{4} \left[ 3\lambda_1 + 4\lambda_2 - \lambda_1 \left( \cos(2\theta_S) - \sqrt{2} \sin(2\theta_S) \right) \right] \\
& + \int_k \tilde{\mathcal{S}}_{(1)}(k) \cdot \frac{3}{2} \left[ \lambda_1 + 2\lambda_2 \right] \\
& + \int_k \tilde{\mathcal{S}}_{(4)}(k) \cdot 3 \left[ \lambda_1 + 2\lambda_2 \right] \\
& + \int_k \tilde{\mathcal{P}}_{(0)}(k) \cdot \frac{1}{12} \left[ 9\lambda_1 + 12\lambda_2 - \lambda_1 \left( 5 \cos(2\theta_P) + \sqrt{2} \sin(2\theta_P) \right) \right] \\
& + \int_k \tilde{\mathcal{P}}_{(8)}(k) \cdot \frac{1}{12} \left[ 9\lambda_1 + 12\lambda_2 + \lambda_1 \left( 5 \cos(2\theta_P) + \sqrt{2} \sin(2\theta_P) \right) \right] \\
& + \int_k \tilde{\mathcal{P}}_{(1)}(k) \cdot \frac{3}{2} \left[ \lambda_1 + 2\lambda_2 \right] \\
& + \int_k \tilde{\mathcal{P}}_{(4)}(k) \cdot \left[ 3\lambda_1 + 4\lambda_2 \right]. \tag{B20}
\end{aligned}$$

For the diagonalized pseudoscalar meson self-energies  $\tilde{\Pi}_{(i)}$ , they are the same as  $\tilde{\Sigma}_{(i)}$  with the replacement

$$\tilde{\mathcal{S}}_{(0)}(k) \longleftrightarrow \tilde{\mathcal{P}}_{(0)}(k) \quad \text{and} \quad \theta_S \longleftrightarrow \theta_P. \tag{B21}$$

We do not show them explicitly for readability.

To obtain the value of the rotation angles  $\theta_{S/P}$  in Eq.(B13), we look at the 08-component of the gap equations in

Eq.(B11) after performing the orthogonal transformation, which turns out to give the following constraints:

$$\begin{aligned} 0 &= \left[ \tilde{m}_S^2(\bar{\sigma}) \right]^{08} + \tilde{\Sigma}^{08}, \\ 0 &= \left[ \tilde{m}_P^2(\bar{\sigma}) \right]^{08} + \tilde{\Pi}^{08}, \end{aligned} \quad (\text{B22})$$

where

$$\left[ \tilde{m}_{S/P}^2(\bar{\sigma}) \right]^{08} = \left[ m_{S/P}^2(\bar{\sigma}) \right]^{08} \cos(2\theta_{S/P}) - \left\{ \left[ m_{S/P}^2(\bar{\sigma}) \right]^{00} - \left[ m_{S/P}^2(\bar{\sigma}) \right]^{88} \right\} \cos(\theta_{S/P}) \sin(\theta_{S/P}), \quad (\text{B23})$$

and

$$\begin{aligned} \tilde{\Sigma}^{08} &= \int_k \tilde{\mathcal{S}}_{(0)}(k) \cdot \frac{\lambda_1}{8} \left[ \sin \theta_S \left( 9 \cos \theta_S + 7 \cos(3\theta_S) - 4\sqrt{2} \sin(3\theta_S) \right) \right] \\ &+ \int_k \tilde{\mathcal{S}}_{(8)}(k) \cdot \frac{\lambda_1}{8} \left[ \cos \theta_S \left( 9 \sin \theta_S - 7 \sin(3\theta_S) - 4\sqrt{2} \cos(3\theta_S) \right) \right] \\ &+ \int_k \tilde{\mathcal{S}}_{(1)}(k) \cdot \frac{3\lambda_1}{4} \left[ 2\sqrt{2} \cos(2\theta_S) - \sin(2\theta_S) \right] \\ &- \int_k \tilde{\mathcal{S}}_{(4)}(k) \cdot \lambda_1 \left[ \sqrt{2} \cos(2\theta_S) + \sin(2\theta_S) \right] \\ &+ \int_k \tilde{\mathcal{P}}_{(0)}(k) \cdot \frac{\lambda_1}{24} \sin \theta_P \left[ 9 \cos(\theta_P - 2\theta_S) + 7 \cos(\theta_P + 2\theta_S) - 4\sqrt{2} \sin(\theta_P + 2\theta_S) \right] \\ &- \int_k \tilde{\mathcal{P}}_{(8)}(k) \cdot \frac{\lambda_1}{24} \cos \theta_P \left[ 9 \sin(\theta_P - 2\theta_S) + 7 \sin(\theta_P + 2\theta_S) + 4\sqrt{2} \cos(\theta_P + 2\theta_S) \right] \\ &+ \int_k \tilde{\mathcal{P}}_{(1)}(k) \cdot \frac{\lambda_1}{4} \left[ 2\sqrt{2} \cos(2\theta_S) - \sin(2\theta_S) \right] \\ &- \int_k \tilde{\mathcal{P}}_{(4)}(k) \cdot \frac{\lambda_1}{3} \left[ \sqrt{2} \cos(2\theta_S) - 5 \sin(2\theta_S) \right]. \end{aligned} \quad (\text{B24})$$

Again, the pseudoscalar mixing self-energy  $\tilde{\Pi}^{08}$  is obtained directly through  $\tilde{\Sigma}^{08}$  simply by the replacement in Eq. (B21).

### 3. The stationary condition for VEVs

The stationary conditions derived from the 2PI effective potential (B1) reads

$$\begin{aligned} 0 &= \frac{\partial V(\bar{\sigma})}{\partial \bar{\sigma}_0} - 3\mathcal{G}^{0bc} \left[ \int_k \mathcal{S}_{cb}(k) - \int_k \mathcal{P}_{cb}(k) \right] + 4\mathcal{F}^{0bcd} \bar{\sigma}_b \int_k \mathcal{S}_{dc}(k) + 4\mathcal{H}^{0bcd} \bar{\sigma}_b \int_k \mathcal{P}_{dc}(k), \\ 0 &= \frac{\partial V(\bar{\sigma})}{\partial \bar{\sigma}_8} - 3\mathcal{G}^{8bc} \left[ \int_k \mathcal{S}_{cb}(k) - \int_k \mathcal{P}_{cb}(k) \right] + 4\mathcal{F}^{8bcd} \bar{\sigma}_b \int_k \mathcal{S}_{dc}(k) + 4\mathcal{H}^{8bcd} \bar{\sigma}_b \int_k \mathcal{P}_{dc}(k), \end{aligned} \quad (\text{B25})$$

where  $V(\bar{\sigma})$  is given in Eq. (A3), and

$$\begin{aligned} \mathcal{G}^{abc} &\equiv -\frac{1}{6} \frac{\partial^3 V_{\text{anom}}}{\partial \sigma_a \partial \sigma_b \partial \sigma_c} \Big|_{\Phi=0} = \frac{1}{6} \frac{\partial^3 V_{\text{anom}}}{\partial \sigma_a \partial \pi_b \partial \pi_c} \Big|_{\Phi=0} \\ &= \frac{B}{6} \left[ d^{abc} - \frac{3}{2} \left( \delta^{a0} d^{0bc} + \delta^{b0} d^{a0c} + \delta^{c0} d^{ab0} \right) + \frac{9}{2} d^{000} \delta^{a0} \delta^{b0} \delta^{c0} \right]. \end{aligned} \quad (\text{B26})$$

To regularize the meson loops, we perform the vacuum-subtraction prescription, such that

$$\begin{aligned} \int_k \tilde{\mathcal{S}}_{(i)}(k) &= \int \frac{d^3 \mathbf{k}}{(2\pi)^3} \frac{1}{\epsilon_{\mathbf{k}}^{S,(i)}} \left( \exp \left\{ \frac{\epsilon_{\mathbf{k}}^{S,(i)}}{T} \right\} - 1 \right)^{-1}, \\ \int_k \tilde{\mathcal{P}}_{(i)}(k) &= \int \frac{d^3 \mathbf{k}}{(2\pi)^3} \frac{1}{\epsilon_{\mathbf{k}}^{P,(i)}} \left( \exp \left\{ \frac{\epsilon_{\mathbf{k}}^{P,(i)}}{T} \right\} - 1 \right)^{-1}, \end{aligned} \quad (\text{B27})$$

where

$$\epsilon_{\mathbf{k}}^{S/P,(i)} \equiv \sqrt{\mathbf{k}^2 + \left[ \tilde{M}_{S/P}^2 \right]_{(i)}}. \quad (\text{B28})$$

## Appendix C: Derivations of WTIs and extension to anomalous WTIs

### 1. Chiral-limit WTIs in 1PI formalism and threshold property of pseudo NG masses

Consider a continuous symmetry ( $\in$  group  $G$ ) associated with the infinitesimal variation ( $\delta_\epsilon$ ) of the field  $\phi$  (in the linear symmetry realization) and the action  $S[\phi]$  as follows:

$$\delta_\epsilon S[\phi] = \frac{\delta S}{\delta \phi_a} \cdot \delta_\epsilon \phi_a = 0, \quad \delta_\epsilon \phi_a = d_a^b \phi_b \quad (\text{C1})$$

where  $d_a^b$  is arbitrary coefficient matrix in the field space, and  $A \cdot B \equiv \int_x A(x)B(x)$ . The generating functional for the action  $S[\phi]$  is defined together with the source  $J_a$  for  $\phi_a$  as

$$Z[J] = \int [\mathcal{D}\phi_a] e^{-S[\phi] + J^a \cdot \phi_a} = e^{W[J]}, \quad (\text{C2})$$

Imposing this  $Z[J]$  to be invariant under the symmetry transformation in Eq.(C1), we have

$$\int [\mathcal{D}\phi'_a] e^{-S[\phi'] + J^a \cdot \phi'_a} \Big|_{\phi'_a = \phi_a + i\epsilon \delta_\epsilon \phi_a} = \int [\mathcal{D}\phi_a] e^{-S[\phi] + J^a \cdot \phi_a}, \quad (\text{C3})$$

Suppose that the path integral measure  $[\mathcal{D}\phi_a]$  is invariant under this symmetry, i.e., not anomaly there, we find the following identity:

$$\begin{aligned} & \int [\mathcal{D}\phi_a] \left[ e^{-S[\phi'] + J^a \cdot \phi'_a} - e^{-S[\phi] + J^a \cdot \phi_a} \right]_{\phi'_a = \phi_a + i\epsilon \delta_\epsilon \phi_a} \\ &= -i\epsilon \int [\mathcal{D}\phi_a] \left[ \frac{\delta S}{\delta \phi_a} \cdot \delta_\epsilon \phi_a - J^a \cdot \delta_\epsilon \phi_a \right] e^{-S[\phi] + J^a \cdot \phi_a} + \mathcal{O}(\epsilon^2) \\ &= i\epsilon \left[ J^a \cdot \langle \delta_\epsilon \phi_a \rangle_J \right] Z[J] + \mathcal{O}(\epsilon^2) \\ &= 0, \end{aligned} \quad (\text{C4})$$

where

$$\langle O \rangle_J \equiv \frac{1}{Z[J, \mathcal{M}]} \int [\mathcal{D}\phi_a] O e^{-S[\phi, \mathcal{M}] + J^a \cdot \phi_a}. \quad (\text{C5})$$

Equation (C4) gives the WTI at the generating functional level,

$$J^a \cdot \langle \delta_\epsilon \phi_a \rangle_J = 0. \quad (\text{C6})$$

Defining the 1PI effective action

$$\Gamma[\phi_{\text{cl}}] = \sup_J \left( J \cdot \phi_{\text{cl}} - W[J] \right), \quad (\text{C7})$$

we have

$$\frac{\delta W}{\delta J^a} = \langle \phi_a \rangle_J \equiv (\phi_{\text{cl}})_a, \quad \frac{\delta \Gamma}{\delta (\phi_{\text{cl}})_a} = J^a. \quad (\text{C8})$$

Replacing  $J_a$  with  $\Gamma$  as above, the WTI in Eq.(C6) is cast into the form

$$\frac{\delta \Gamma}{\delta (\phi_{\text{cl}})_a} \cdot \delta_\epsilon (\phi_{\text{cl}})_a = 0, \quad (\text{C9})$$



where  $\delta_\epsilon(\phi_{\text{cl}})_a = d_a^b(\phi_{\text{cl}})_b$ .

We apply the WTI arguments above into the present LSM case. First of all, consider the chiral limit. In the chiral limit, the LSM action is invariant under the chiral  $SU(3)_L \times SU(3)_R$  transformation,

$$\Phi \rightarrow g_L \cdot \Phi \cdot g_R^\dagger, \quad (\text{C10})$$

with  $g_{L/R} = \exp\{i(\theta_{L/R})_\alpha T^\alpha\}$  and  $\alpha = 1, \dots, 8$ . Under the  $SU(3)$  axial rotation with  $(\theta_L)_\alpha = -(\theta_R)_\alpha = (\theta_A)_\alpha$ , the  $\sigma_a$  and  $\pi_a$  thus infinitesimally transform like

$$\begin{aligned} \delta^\alpha(\sigma_a T^a) &= \{T^\alpha, \pi_a T^a\}, \\ \delta^\alpha(\pi_a T^a) &= -\{T^\alpha, \sigma_a T^a\}, \end{aligned} \quad (\text{C11})$$

Or equivalently,

$$\delta^\alpha \sigma_a = d^{\alpha b}{}_a \pi_b, \quad \delta^\alpha \pi_a = -d^{\alpha b}{}_a \sigma_b, \quad (\text{C12})$$

where

$$d^{\alpha b}{}_a \equiv 2 \text{tr} \left[ \{T^\alpha, T^b\} T_a \right], \quad d^{\alpha b}{}_0 = \sqrt{\frac{2}{3}} \delta^{\alpha b}. \quad (\text{C13})$$

When the general WTI in Eq.(C9) is applied to the 1PI effective action in the LSM, we have

$$0 = \frac{\delta\Gamma[\sigma_{\text{cl}}, \pi_{\text{cl}}]}{\delta(\sigma_{\text{cl}})_a} \cdot \delta^\alpha(\sigma_{\text{cl}})_a + \frac{\delta\Gamma[\sigma_{\text{cl}}, \pi_{\text{cl}}]}{\delta(\pi_{\text{cl}})_a} \cdot \delta^\alpha(\pi_{\text{cl}})_a = \frac{\delta\Gamma[\sigma_{\text{cl}}, \pi_{\text{cl}}]}{\delta(\sigma_{\text{cl}})_a} \cdot d^{\alpha b}{}_a (\pi_{\text{cl}})_b + \frac{\delta\Gamma[\sigma_{\text{cl}}, \pi_{\text{cl}}]}{\delta(\pi_{\text{cl}})_a} \cdot d^{\alpha b}{}_a (\sigma_{\text{cl}})_b. \quad (\text{C14})$$

Performing one more functional derivative with respect to the external (background) pseudoscalar field  $(\pi_{\text{cl}}(y))_{b_1}$  on the WTIs in Eq.(C14), we get

$$\begin{aligned} & \frac{\delta}{\delta(\pi_{\text{cl}}(y))_{b_1}} \left( \frac{\delta\Gamma[\sigma_{\text{cl}}, \pi_{\text{cl}}]}{\delta(\sigma_{\text{cl}})_a} \cdot d^{\alpha b}{}_a (\pi_{\text{cl}})_b + \frac{\delta\Gamma[\sigma_{\text{cl}}, \pi_{\text{cl}}]}{\delta(\pi_{\text{cl}})_a} \cdot d^{\alpha b}{}_a (\sigma_{\text{cl}})_b \right) \\ &= \frac{\delta\Gamma}{\delta(\sigma_{\text{cl}})_a} \cdot \delta^{(4)}(x-y) d^{\alpha b_1}{}_a - \frac{\delta^2\Gamma}{\delta(\pi_{\text{cl}}(y))_{b_1} \delta(\pi_{\text{cl}}(x))_a} \cdot d^{\alpha b}{}_a (\sigma_{\text{cl}})_b. \end{aligned} \quad (\text{C15})$$

Imposing the quantum equations of motion such that  $\frac{\delta\Gamma}{\delta(\sigma_{\text{cl}})_a} = 0$  at the background field values  $\bar{\Phi}$ , Eq.(C15) is simplified to

$$-\frac{\delta^2\Gamma}{\delta(\pi_{\text{cl}}(y))_{b_1} \delta(\pi_{\text{cl}}(x))_a} \cdot d^{\alpha b}{}_a \bar{\sigma}_b = -\int_x \left[ \mathcal{P}^{-1}(y, x) \right]^{b_1 a} d^{\alpha b}{}_a \bar{\sigma}_b, \quad (\text{C16})$$

where  $(\mathcal{P}^{-1}(y, x))^{b_1 a}$  is the full inverse propagator of the pseudoscalar mesons satisfying the gap equations in Eq.(B4). In the present system, the translation invariance holds when we turn off the external sources, thus in Euclidean momentum space,  $(\mathcal{P}^{-1}(y, x))^{b_1 a}$  can be Fourier transformed like

$$\left[ \mathcal{P}^{-1}(y, x) \right]^{b_1 a} = \int \frac{d^4 k}{(2\pi)^4} \left[ \mathcal{P}^{-1}(k) \right]^{b_1 a} e^{i(y-x) \cdot k}. \quad (\text{C17})$$

In the Hartree approximation, as done in Eq.(B10),  $\mathcal{P}^{-1}(k)$  can have momentum dependence only from the canonical kinetic part as

$$\left[ \mathcal{P}^{-1}(k) \right]^{b_1 a} = k^2 \delta^{b_1 a} + \left[ M_P^2 \right]^{b_1 a}. \quad (\text{C18})$$

Putting Eqs.(C17) and (C18) into Eq.(C16), we are able to perform the above  $x$ -integral in Eq.(C16), to get

$$\begin{aligned} -\int_x \left[ \mathcal{P}^{-1}(y, x) \right]^{b_1 a} d^{\alpha b}{}_a \bar{\sigma}_b &= -\int d^4 x \int \frac{d^4 k}{(2\pi)^4} \left[ \mathcal{P}^{-1}(k) \right]^{b_1 a} e^{i(y-x) \cdot k} d^{\alpha b}{}_a \bar{\sigma}_b \\ &= -\left[ \mathcal{P}^{-1}(0) \right]^{b_1 a} d^{\alpha b}{}_a \bar{\sigma}_b \\ &= -\left[ M_P^2 \right]^{b_1 a} d^{\alpha b}{}_a \bar{\sigma}_b. \end{aligned} \quad (\text{C19})$$

Taking  $b_1 = 1$  in Eq.(C19), we find the right hand side to be

$$-\left[M_P^2\right]^{1a} d^{\alpha b}{}_a (\bar{\sigma}_0 \delta_{0b} + \bar{\sigma}_8 \delta_{8b}). \quad (C20)$$

Since the  $SU(3)$  vectorial symmetry is present in the system, the  $SU(2)$  triplet pions and the  $SU(2)$  doublet kaons do not mix each other, hence we have  $\left[M_P^2\right]^{1a} = \left[M_P^2\right]^{11} \delta^{1a}$ . Noting also that  $d^{\alpha 0}{}_1 = \sqrt{2/3} \delta_1^\alpha$  and  $d^{\alpha 8}{}_1 = 1/\sqrt{3} \delta_1^\alpha$ , we then get

$$-\left[M_P^2\right]^{11} d^{\alpha b}{}_1 (\bar{\sigma}_0 \delta_{0b} + \bar{\sigma}_8 \delta_{8b}) = -M_\pi^2 \left( \sqrt{\frac{2}{3}} \bar{\sigma}_0 + \frac{1}{\sqrt{3}} \bar{\sigma}_8 \right) \delta_1^\alpha = -2M_\pi^2 \bar{\Phi}_1 \delta_1^\alpha. \quad (C21)$$

By taking  $b_1 = 4$  in Eq.(C19), the right hand side is evaluated to be

$$-\left[M_P^2\right]^{44} d^{\alpha b}{}_4 (\bar{\sigma}_0 \delta_{0b} + \bar{\sigma}_8 \delta_{8b}). \quad (C22)$$

Here, we have  $d^{\alpha 0}{}_4 = \sqrt{2/3} \delta_0^\alpha$  and  $d^{\alpha 8}{}_4 = -1/(2\sqrt{3}) \delta_4^\alpha$ , such that

$$-\left[M_P^2\right]^{44} d^{\alpha b}{}_4 (\bar{\sigma}_0 \delta_{0b} + \bar{\sigma}_8 \delta_{8b}) = -M_\kappa^2 \left( \sqrt{\frac{2}{3}} \bar{\sigma}_0 - \frac{1}{2\sqrt{3}} \bar{\sigma}_8 \right) \delta_4^\alpha = -M_\kappa^2 (\bar{\Phi}_1 + \bar{\Phi}_3) \delta_4^\alpha. \quad (C23)$$

Taking  $\alpha = 1$  and  $\alpha = 4$  individually, we thus find the following threshold property for the pion and kaon masses

$$M_\pi^2 \bar{\Phi}_1 = 0, \quad M_\kappa^2 (\bar{\Phi}_1 + \bar{\Phi}_3) = 0, \quad (C24)$$

which precisely follows the massless NG boson when  $\bar{\Phi}_1$  or  $\bar{\Phi}_8$  takes nonzero, i.e., the spontaneous breaking of the chiral symmetry takes place.

## 2. Anomalous WTIs and GOR relations

In the present LSM, actually, the chiral  $SU(3)$  symmetry is explicitly broken by the current quark masses encoded in the spurion field  $\mathcal{M}$ . We therefore extend the formulation described above on the chiral-limit WTIs by including  $\mathcal{M}$ .

As in the main text, the spurion field  $\mathcal{M}$  is introduced so as to compensate the explicit chiral breaking by quark masses in the action. The spurion field  $\mathcal{M}$  therefore transforms under the chiral  $SU(3)$  symmetry in the same way as  $\phi$  does in Eq.(C10):

$$\mathcal{M} \rightarrow g_L \cdot \mathcal{M} \cdot g_R^\dagger. \quad (C25)$$

Thus the chiral variation of the action, as generically given in Eq.(C1), gets shifted as

$$\delta_\epsilon S[\phi] = \frac{\delta S}{\delta \phi_a} \cdot \delta_\epsilon \phi_a + \frac{\delta S}{\delta \mathcal{M}} \cdot \delta_\epsilon \mathcal{M} + \frac{\delta S}{\delta \mathcal{M}^\dagger} \cdot \delta_\epsilon \mathcal{M}^\dagger = 0. \quad (C26)$$

In the generating functional level level, Eq. (C4) is then also modified to be like

$$\begin{aligned} & \int [\mathcal{D}\phi_a] \left[ e^{-S[\phi', \mathcal{M}] + J^a \cdot \phi'_a} - e^{-S[\phi, \mathcal{M}] + J^a \cdot \phi_a} \right]_{\phi'_a = \phi_a + i\epsilon \delta_\epsilon \phi_a} \\ &= -i\epsilon \int [\mathcal{D}\phi_a] \left[ \frac{\delta S}{\delta \phi_a} \cdot \delta_\epsilon \phi_a - J^a \cdot \delta_\epsilon \phi_a \right] e^{-S[\phi, \mathcal{M}] + J^a \cdot \phi_a} + \mathcal{O}(\epsilon^2) \\ &= i\epsilon \int [\mathcal{D}\phi_a] \left[ \frac{\delta S}{\delta \mathcal{M}} \cdot \delta_\epsilon \mathcal{M} + \frac{\delta S}{\delta \mathcal{M}^\dagger} \cdot \delta_\epsilon \mathcal{M}^\dagger + J^a \cdot \delta_\epsilon \phi_a \right] e^{-S[\phi, \mathcal{M}] + J^a \cdot \phi_a} + \mathcal{O}(\epsilon^2) \\ &= i\epsilon \left[ \left\langle \frac{\delta S}{\delta \mathcal{M}} \right\rangle_J \cdot \delta_\epsilon \mathcal{M} + \left\langle \frac{\delta S}{\delta \mathcal{M}^\dagger} \right\rangle_J \cdot \delta_\epsilon \mathcal{M}^\dagger + J^a \cdot \langle \delta_\epsilon \phi_a \rangle_J \right] Z[J, \mathcal{M}] + \mathcal{O}(\epsilon^2) \\ &= 0. \end{aligned} \quad (C27)$$

We then find the general form of the anomalous WTIs inclding  $\mathcal{M}$ ,

$$\left\langle \frac{\delta S}{\delta \mathcal{M}} \right\rangle_J \cdot \delta_\epsilon \mathcal{M} + \left\langle \frac{\delta S}{\delta \mathcal{M}^\dagger} \right\rangle_J \cdot \delta_\epsilon \mathcal{M}^\dagger + J^a \cdot \langle \delta_\epsilon \phi_a \rangle_J = 0. \quad (\text{C28})$$

Written in terms of the 1PI effective action in Eq.(C7), the anomalous WTIs take the form

$$\frac{\delta S}{\delta \mathcal{M}} \bigg|_{\phi_a = (\phi_{\text{cl}})_a + \Delta_{ab} \cdot \frac{\delta}{\delta (\phi_{\text{cl}})_b}} \cdot \delta_\epsilon \mathcal{M} + \frac{\delta S}{\delta \mathcal{M}^\dagger} \bigg|_{\phi_a = (\phi_{\text{cl}})_a + \Delta_{ab} \cdot \frac{\delta}{\delta (\phi_{\text{cl}})_b}} \cdot \delta_\epsilon \mathcal{M}^\dagger + \frac{\delta \Gamma}{\delta (\phi_{\text{cl}})_a} \cdot \delta_\epsilon (\phi_{\text{cl}})_a = 0, \quad (\text{C29})$$

where

$$\Delta_{ab}(x, y) = \frac{\delta^2 W}{\delta J(x) \delta J(y)} \quad (\text{C30})$$

denotes the full connected two-point function.

With Eq. (C29) at hand, we are ready to derive the GOR relations at the 1PI level. In the last subsection, we have dealt with the first term in Eq. (C29), hence, we focus on the latter two terms. Following Eq.(C25) The infinitesimal transformation of  $\mathcal{M}$  goes like

$$\delta^\alpha \mathcal{M}_{mn} = \{T^\alpha, \mathcal{M}\}_{mn}. \quad (\text{C31})$$

Decomposing  $\mathcal{M}$  into scalar and pseudoscalar parts as  $\mathcal{M} = \mathcal{M}^s + i\mathcal{M}^p = \mathcal{M}_a^s T^a + i\mathcal{M}_a^p T^a$ , the transformation of  $\mathcal{M}_a^{s/p}$  then reads as

$$\delta^\alpha \mathcal{M}_a^s = d^{\alpha b}{}_a \mathcal{M}_b^p, \quad \delta^\alpha \mathcal{M}_a^p = -d^{\alpha b}{}_a \mathcal{M}_b^s. \quad (\text{C32})$$

Consider

$$\begin{aligned} \frac{\delta S_{\text{LSM}}}{\delta \mathcal{M}_{mn}} &= -c(\Phi^\dagger)_{nm} - kc\epsilon_{mbc}\epsilon^{nef}\Phi_e^b\Phi_f^c \\ &= -c(\sigma_a - i\pi_a)T_{nm}^a - kc(\sigma_{a_1} + i\pi_{a_1})(\sigma_{a_2} + i\pi_{a_2})\epsilon_{mbc}\epsilon^{nef}(T^{a_1})_e^b(T^{a_2})_f^c. \end{aligned} \quad (\text{C33})$$

Replacing  $\phi_a$  by  $(\phi_{\text{cl}})_a + \Delta_{ab} \cdot \frac{\delta}{\delta (\phi_{\text{cl}})_b}$ , we obtain

$$\begin{aligned} \frac{\delta S_{\text{LSM}}}{\delta \mathcal{M}_{mn}} \bigg|_{\phi_a = (\phi_{\text{cl}})_a + \Delta_{ab} \cdot \frac{\delta}{\delta (\phi_{\text{cl}})_b}} \cdot \delta^\alpha \mathcal{M}_{mn} &= -c \left[ (\sigma_{\text{cl}})_a - i(\pi_{\text{cl}})_a \right] \cdot \left[ \mathcal{M}_{a_2}^p - i\mathcal{M}_{a_2}^s \right] T_{nm}^b T_{nm}^a d^{\alpha a_2}{}_b \\ &\quad - kc \left[ \mathcal{S}_{a_1 a_2}(x, x) + i\mathcal{P}_{a_1 a_2}(x, x) \right] \cdot \left[ \mathcal{M}_{a_3}^p - i\mathcal{M}_{a_3}^s \right] \epsilon_{mbc}\epsilon^{nef}(T^g)_n^m (T^{a_1})_e^b (T^{a_2})_f^c d^{\alpha a_3}{}_g \\ &\quad - kc \left[ (\sigma_{\text{cl}})_{a_1} (\sigma_{\text{cl}})_{a_2} + i(\sigma_{\text{cl}})_{a_1} (\pi_{\text{cl}})_{a_2} + i(\pi_{\text{cl}})_{a_1} (\sigma_{\text{cl}})_{a_2} - (\pi_{\text{cl}})_{a_1} (\pi_{\text{cl}})_{a_2} \right] \cdot \left[ \mathcal{M}_{a_3}^p - i\mathcal{M}_{a_3}^s \right] \\ &\quad \times \epsilon_{mbc}\epsilon^{nef}(T^g)_n^m (T^{a_1})_e^b (T^{a_2})_f^c d^{\alpha a_3}{}_g, \end{aligned} \quad (\text{C34})$$

where  $\mathcal{S}_{a_1 a_2}(x, y)$  and  $\mathcal{P}_{a_1 a_2}(x, y)$  are the full-dressed scalar and pseudoscalar propagators. We further get the following.

$$\begin{aligned} &\frac{\delta}{\delta (\pi_{\text{cl}}(y))_{b_1}} (\text{C34}) \\ &= c\delta^{(4)}(x-y) \left[ \delta_{a_1}^{b_1} \right] \cdot \left[ \mathcal{M}_{a_2}^s + i\mathcal{M}_{a_2}^p \right] T_{mn}^b T_{nm}^a d^{\alpha a_2}{}_b \\ &\quad - kc \left[ \frac{\delta}{\delta (\pi_{\text{cl}}(y))_{b_1}} \mathcal{S}_{a_1 a_2}(x, x) + i \frac{\delta}{\delta (\pi_{\text{cl}}(y))_{b_1}} \mathcal{P}_{a_1 a_2}(x, x) \right] \cdot \left[ \mathcal{M}_{a_3}^p - i\mathcal{M}_{a_3}^s \right] \\ &\quad \times \epsilon_{mbc}\epsilon^{nef}(T^g)_n^m (T^{a_1})_e^b (T^{a_2})_f^c d^{\alpha a_3}{}_g \\ &\quad - kc\delta^{(4)}(x-y) \left[ \left( (\sigma_{\text{cl}})_{a_1} + i(\pi_{\text{cl}})_{a_1} \right) \delta_{a_2}^{b_1} + \delta_{a_1}^{b_1} \left( (\sigma_{\text{cl}})_{a_2} + i(\pi_{\text{cl}})_{a_2} \right) \right] \cdot \left[ \mathcal{M}_{a_3}^s + i\mathcal{M}_{a_3}^p \right] \end{aligned}$$

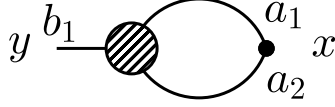


FIG. 6. A Feynman diagram of the meson scattering kernel defined in Eq. (C37). The solid line connected to the point  $y$  denotes the pseudoscalar meson propagator, and the lines involving the point  $x$  represent the scalar or pseudoscalar meson propagators. The hatched blob stands for the dressed three-point meson vertex in the 1PI formulation.

$$\begin{aligned}
& \times \epsilon_{mbc} \epsilon^{nef} (T^g)_n^m (T^{a_1})_e^b (T^{a_2})_f^c d^{\alpha a_3}_g \\
& = \frac{c}{2} \delta^{(4)}(x-y) \left[ \delta_a^{b_1} \right] \cdot \left[ \mathcal{M}_{a_2}^s + i \mathcal{M}_{a_2}^p \right] \delta^{ab} d^{\alpha a_2}_b \\
& \quad - k c \left[ H_{a_1 a_2}^{b_1}(y, x) \right] \cdot \left[ \mathcal{M}_{a_3}^p - i \mathcal{M}_{a_3}^s \right] \mathcal{T}^{g a_1 a_2} d^{\alpha a_3}_g \\
& \quad - k c \delta^{(4)}(x-y) \left[ \left( (\sigma_{\text{cl}})_{a_1} + i(\pi_{\text{cl}})_{a_1} \right) \delta_{a_2}^{b_1} + \delta_{a_1}^{b_1} \left( (\sigma_{\text{cl}})_{a_2} + i(\pi_{\text{cl}})_{a_2} \right) \right] \cdot \left[ \mathcal{M}_{a_3}^s + i \mathcal{M}_{a_3}^p \right] \mathcal{T}^{g a_1 a_2} d^{\alpha a_3}_g, \quad (\text{C35})
\end{aligned}$$

where

$$\mathcal{T}^{g a_1 a_2} \equiv \epsilon_{mbc} \epsilon^{nef} (T^g)_n^m (T^{a_1})_e^b (T^{a_2})_f^c. \quad (\text{C36})$$

In Eq.(C35), we have defined the *meson scattering kernel*  $H_{a_1 a_2}^{b_1}(y, x)$  as

$$H_{a_1 a_2}^{b_1}(y, x) \equiv \frac{\delta}{\delta(\pi_{\text{cl}}(y))_{b_1}} \mathcal{S}_{a_1 a_2}(x, x) + i \frac{\delta}{\delta(\pi_{\text{cl}}(y))_{b_1}} \mathcal{P}_{a_1 a_2}(x, x). \quad (\text{C37})$$

The corresponding diagrammatic interpretation is available in Fig. 6.

The meson scattering kernel  $H_{a_1 a_2}^{b_1}(y, x)$  includes the fully dressed 3-point meson vertex. In the present work, we adopt the truncation scheme such that the 3-point meson vertex is replaced by the tree-level vertex, i.e.,

$$\frac{\delta^3 \Gamma}{\delta \sigma_a(x) \delta \sigma_b(y) \delta \sigma_c(z)} = - \frac{\delta^3 \Gamma}{\delta \sigma_a(x) \delta \pi_b(y) \delta \pi_c(z)} = \frac{\delta^3 S_{\text{LSM}}}{\delta \sigma_a(x) \delta \sigma_b(y) \delta \sigma_c(z)} = -6 \mathcal{G}^{abc} \delta^{(4)}(x-y) \delta^{(4)}(x-z), \quad (\text{C38})$$

where  $\mathcal{G}^{abc}$  is defined in Eq. (B26). We find that within the current truncation scheme, the contribution from the meson scattering kernel vanishes in the anomalous WTIs, in Eq.(C35).

Taking the background field values  $\bar{\sigma}_a T^a = \text{diag}\{\bar{\Phi}_1, \bar{\Phi}_1, \bar{\Phi}_3\}$ ,  $\mathcal{M} = \text{diag}\{m_l, m_l, m_s\}$ , and  $\bar{\pi}_a = 0$ , we see that for  $b_1 = \alpha = 1$ ,

$$(\text{C35}) = c m_l + 2 k c m_l \bar{\Phi}_3, \quad (\text{C39})$$

and for  $b_1 = \alpha = 4$ ,

$$(\text{C35}) = \frac{1}{2} (c m_l + c m_s) + k (c m_l + c m_s) \bar{\Phi}_1, \quad (\text{C40})$$

where we have integrated spacetime over  $x$ . The hermitian conjugated term  $\propto \mathcal{M}^\dagger$  gives the same result as above.

Combining Eqs. (C21), (C23), (C39), and (C40), we get the GOR relations expressed in terms of the LSM parameters, as in Eq.(27),

$$\begin{aligned}
M_\pi^2 \bar{\Phi}_1 &= c m_l (1 + 2 k \bar{\Phi}_3), \\
M_\kappa^2 (\bar{\Phi}_1 + \bar{\Phi}_3) &= (c m_l + c m_s) (1 + 2 k \bar{\Phi}_1). \quad (\text{C41})
\end{aligned}$$

These two relations coincide with those obtained from the tree-level action, as we expected, meaning that the contributions to the explicit chiral breaking terms generated from the quantum fluctuations are dropped in the current truncation scheme. In the 1PI formulation, the above GOR relations are actually equivalent to the stationary conditions for  $\bar{\Phi}_1$  and  $\bar{\Phi}_3$ , which substantially deviates from each other in the 2PI formalism, as noted in the main text and will be more clarified in the next section.

### 3. (Anomalous) WTIs in 2PI formalism

Considering the generating functional with a bilocal source  $K^{ab}(x, y)$ ,

$$Z[J, K] = \int [\mathcal{D}\phi_a] e^{-S[\phi] + J^a \cdot \phi_a + \frac{1}{2} \phi_a \cdot K^{ab} \cdot \phi_b} = e^{W[J, K]}, \quad (\text{C42})$$

we have

$$\frac{\delta W[J, K]}{\delta J^a} = \langle \phi_a \rangle_{J, K} \equiv (\phi_{\text{cl}})_a, \quad \frac{\delta W}{\delta J^a \delta J^b} = \langle \phi_a \phi_b \rangle_{J, K} - \langle \phi_a \rangle_{J, K} \langle \phi_b \rangle_{J, K} \equiv \Delta_{ab}, \quad (\text{C43})$$

and

$$\frac{\delta W[J, K]}{\delta K^{ab}} = \frac{1}{2} \left( \Delta_{ab} + (\phi_{\text{cl}})_a (\phi_{\text{cl}})_b \right). \quad (\text{C44})$$

The 2PI effective action is obtained by performing the following double-Legendre transformation:

$$\begin{aligned} \Gamma[\phi_{\text{cl}}, \Delta] &= \sup_K \left[ K^{ab} \cdot \frac{\delta \Gamma[\phi_{\text{cl}}, K]}{\delta K^{ab}} - \sup_J \left( J^a \cdot (\phi_{\text{cl}})_a - W[J, K] \right) \right] \\ &= \sup_K \inf_J \left[ W[J, K] - J^a \cdot (\phi_{\text{cl}})_a - \frac{1}{2} K^{ab} \cdot \left( \Delta_{ab} + (\phi_{\text{cl}})_a (\phi_{\text{cl}})_b \right) \right], \end{aligned} \quad (\text{C45})$$

where we have used

$$\frac{\delta \Gamma[\phi_{\text{cl}}, K]}{\delta K^{ab}} = -\frac{\delta W[J, K]}{\delta K^{ab}}. \quad (\text{C46})$$

We then have

$$\frac{\delta \Gamma[\phi_{\text{cl}}, \Delta]}{\delta (\phi_{\text{cl}})_a} = -J^a - K^{ab} \cdot (\phi_{\text{cl}})_b, \quad \frac{\delta \Gamma[\phi_{\text{cl}}, \Delta]}{\delta \Delta_{ab}} = -\frac{1}{2} K^{ab}. \quad (\text{C47})$$

In a manner simialr to what has been done in Eq. (C4), the symmetry variation as in Eq. (C1) and its invariance of the generating functional  $Z[J, K]$  in Eq.(C42) leads to the WTIs in terms of  $Z[J, K]$ ,

$$\begin{aligned} & \int [\mathcal{D}\phi_a] \left[ e^{-S[\phi'] + J^a \cdot \phi'_a + \frac{1}{2} \phi'_a \cdot K^{ab} \cdot \phi'_b} - e^{-S[\phi] + J^a \cdot \phi_a + \frac{1}{2} \phi_a \cdot K^{ab} \cdot \phi_b} \right] \\ &= -i\epsilon \int [\mathcal{D}\phi_a] \left[ \frac{\delta S}{\delta \phi_a} \cdot \delta_\epsilon \phi_a - J^a \cdot \delta_\epsilon \phi_a - \frac{1}{2} \phi_a \cdot K^{ab} \cdot \delta_\epsilon \phi_b - \frac{1}{2} \delta_\epsilon \phi_a \cdot K^{ab} \cdot \phi_b \right] e^{-S[\phi] + J^a \cdot \phi_a + \frac{1}{2} \phi_a \cdot K^{ab} \cdot \phi_b} \\ & \quad + \mathcal{O}(\epsilon^2) \\ &= i\epsilon \left[ J^a \cdot \langle \delta_\epsilon \phi_a \rangle + \frac{1}{2} K^{ab} \cdot \langle \phi_a \cdot \delta_\epsilon \phi_b \rangle + \frac{1}{2} K^{ab} \cdot \langle \delta_\epsilon \phi_a \cdot \phi_b \rangle \right] Z[J, K] + \mathcal{O}(\epsilon^2) \\ &= 0. \end{aligned} \quad (\text{C48})$$

Taking into account Eqs.(C43) and (C47), we rewrite Eq.(C48) into the form

$$\frac{\delta \Gamma[\phi_{\text{cl}}, \Delta]}{\delta (\phi_{\text{cl}})_a} \cdot d_a^b (\phi_{\text{cl}})_b + \frac{\delta \Gamma[\phi_{\text{cl}}, \Delta]}{\delta \Delta_{ab}} \cdot \left( d_b^c \Delta_{ac} + d_a^c \Delta_{cb} \right) = 0. \quad (\text{C49})$$

This is the exact form of WTIs in the 2PI formalism. Taking the functional derivative of both sides in Eq.(C49) with respect to  $(\phi_{\text{cl}})_c$ , we reach the form of Eq.(32) in the main text:

$$\frac{\delta^2 \Gamma[\phi_{\text{cl}}, \Delta]}{\delta (\phi_{\text{cl}})_c \delta (\phi_{\text{cl}})_a} \cdot d_a^b (\phi_{\text{cl}})_b + \frac{\delta \Gamma[\phi_{\text{cl}}, \Delta]}{\delta (\phi_{\text{cl}})_a} \cdot d_a^c + \frac{\delta^2 \Gamma[\phi_{\text{cl}}, \Delta]}{\delta (\phi_{\text{cl}})_c \delta \Delta_{ab}} \cdot \left( d_b^c \Delta_{ac} + d_a^c \Delta_{cb} \right) = 0. \quad (\text{C50})$$

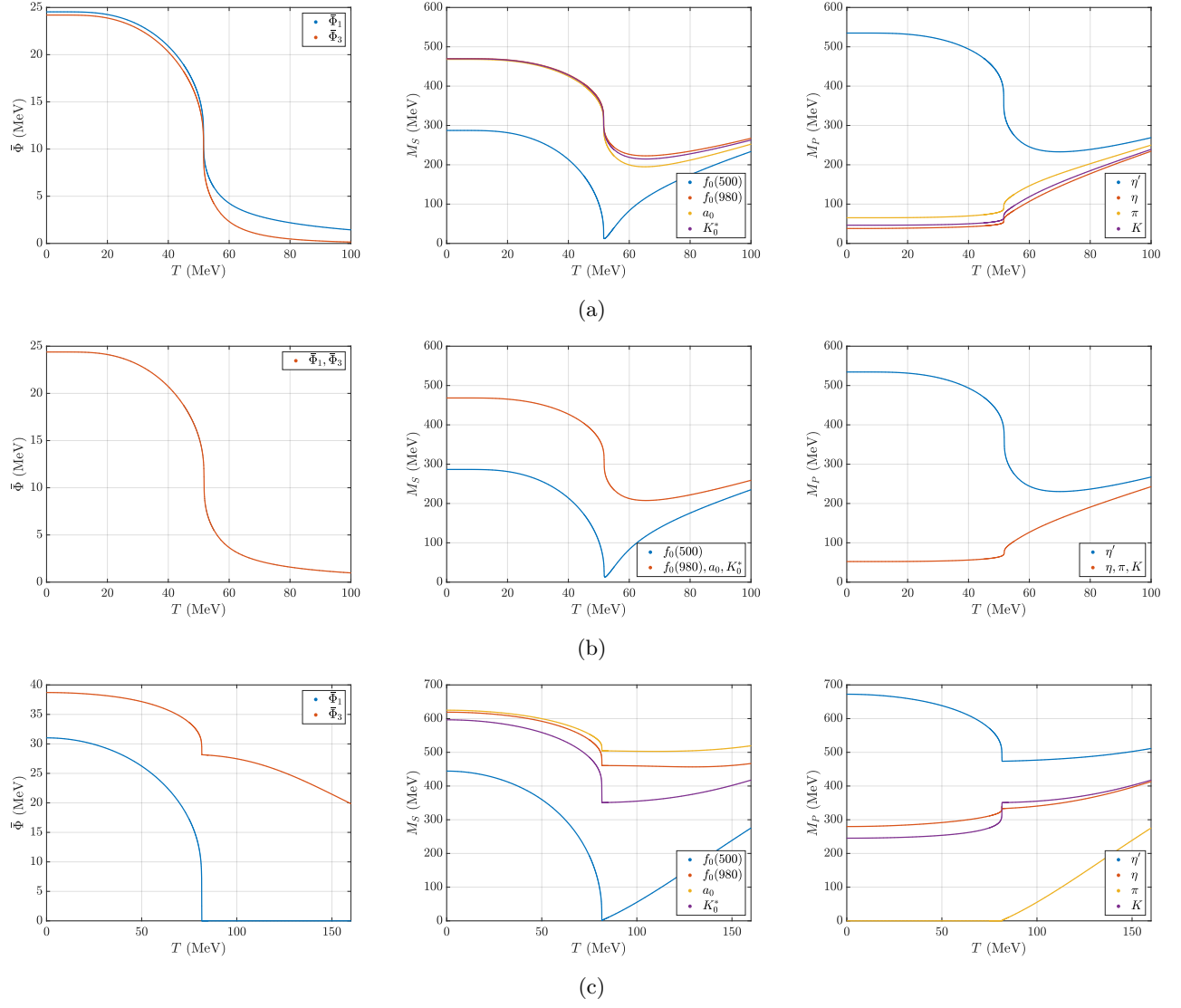


FIG. 7. Benchmarked chiral phase transitions at critical points (a), (b), and (c) defined in the text.

#### Appendix D: Thermal evolutions of chiral order parameters and meson masses at critical points

In this appendix, we present the results based on the SICJT formalism on the  $T$ -dependences of the chiral order parameters  $\bar{\Phi}_{1,3}$  and scalar and pseudoscalar meson masses at several critical points in the Columbia plot, as seen in Fig. 5. We take the parameter set I in Sec. IV B 1 to fix the  $f_0(500)$  mass:  $m[f_0(500)] = 672.4$  MeV.

The chosen critical points are:

- (a)  $(m_l, m_s)/m_l^{\text{phys.}} \simeq (0.1469, 0)$ : the second-order critical line on the  $m_l$ -axis ,
- (b)  $(m_l, m_s)/m_l^{\text{phys.}} \simeq (0.0939, 0.0939)$ : the second-order critical line on the three-flavor symmetric curve ,
- (c)  $(m_l, m_s)/m_s^{\text{phys.}} \simeq (0, 0.175) \simeq (0, m_s^{\text{tri}})/m_s^{\text{phys.}}$ : the second-order critical line on the  $m_s$ -axis, i.e., vicinity of the tricritical point.

In Fig. 7, we plot the  $T$ -dependences of the chiral order parameters  $\bar{\Phi}_{1,3}$  and scalar and pseudoscalar meson masses at those critical points.

The scaling behavior of the light quark condensate  $\langle \bar{\ell}\ell \rangle$  with respect to the temperature  $T$  and the current quark mass  $m_l$  in the vicinity of the criticality is characterized by the critical exponents  $\beta$  and  $\delta$ . Suppose the criticality

Model	$\beta$	$\delta$	$m_\pi$ (MeV)	$T_c$ (MeV)
SICJT: ( $m_l^c = 0.1469 m_l^{\text{phys.}}$ , $m_s^c = 0$ )	0.3618	3.0376	65.3	51.6
SICJT: ( $m_l^c = m_s^c = 0.0939 m_l^{\text{phys.}}$ )	0.3883	2.7442	52.4	51.7
SICJT: ( $m_l^{\text{tri}} = 0$ , $m_s^{\text{tri}} = 0.175 m_s^{\text{phys.}}$ )	0.2286	9.2412	0.0	81.7
SICJT: ( $m_l^c = 0$ , $m_s^c = 2 m_s^{\text{phys.}}$ )	0.3742	7.4033	0.0	155.6
$O(4)$ universality class [60]	0.38	4.82	-	-
$Z_2$ universality class [61]	0.326	4.78	-	-
3D XY universality class [62]	0.3490	4.7798	-	-

TABLE I. The list of the critical exponents at several critical points estimated from the present LSM based on the SICJT formalism with the parameter set I in Sec. IV B 1. The resulting numbers are compared to those from typical statistical models, referred to those critical points when specified;  $O(4)$ ,  $Z_2$ , and 3D XY-universality classes. Also have been shown the corresponding pion mass  $m_\pi$  at the vacuum and the critical temperatures  $T_c$  at the criticalities observed in the present SICJT formalism (See also the bottom-left panel in Fig. 5).

is located at  $(T, m_l) = (T^c, m_l^c)$  with the critical current mass for the strange quark,  $m_s^c$ , we define the following dimensionless variables as

$$t \equiv \frac{T - T^c}{T^c}, \quad \tilde{m}_l \equiv \frac{m_l - m_l^c}{m_l^{\text{phys.}}} . \quad (\text{D1})$$

We also have

$$\langle \bar{\ell} \ell \rangle(t, \tilde{m}_l) - \langle \bar{\ell} \ell \rangle(0, 0) = f_l(t, \tilde{m}_l), \quad (\text{D2})$$

where  $f_l(t, \tilde{m}_l)$  is a dimensionful function and satisfies  $f_l(0, 0) = 0$ . The critical exponents are then given by

$$f_l(t \rightarrow 0, 0) \propto (-t)^\beta, \quad f_l(0, \tilde{m}_l \rightarrow 0) \propto \tilde{m}_l^{1/\delta}. \quad (\text{D3})$$

We list the critical exponents at several critical points in Table. I.

- 
- [1] STAR collaboration, M. M. Aggarwal et al., *An Experimental Exploration of the QCD Phase Diagram: The Search for the Critical Point and the Onset of De-confinement*, [1007.2613](#).
- [2] STAR collaboration, B. Mohanty, *STAR experiment results from the beam energy scan program at RHIC*, *J. Phys. G* **38** (2011) 124023 [[1106.5902](#)].
- [3] X. Luo and N. Xu, *Search for the QCD Critical Point with Fluctuations of Conserved Quantities in Relativistic Heavy-Ion Collisions at RHIC : An Overview*, *Nucl. Sci. Tech.* **28** (2017) 112 [[1701.02105](#)].
- [4] T. Nonaka, *Studying the QCD Phase Diagram in RHIC-BES at STAR*, *JPS Conf. Proc.* **26** (2019) 024007.
- [5] M. Buballa, *NJL model analysis of quark matter at large density*, *Phys. Rept.* **407** (2005) 205 [[hep-ph/0402234](#)].
- [6] K. Fukushima and C. Sasaki, *The phase diagram of nuclear and quark matter at high baryon density*, *Prog. Part. Nucl. Phys.* **72** (2013) 99 [[1301.6377](#)].
- [7] M. Oertel, M. Hempel, T. Klähn and S. Typel, *Equations of state for supernovae and compact stars*, *Rev. Mod. Phys.* **89** (2017) 015007 [[1610.03361](#)].
- [8] PLANCK collaboration, N. Aghanim et al., *Planck 2018 results. VI. Cosmological parameters*, *Astron. Astrophys.* **641** (2020) A6 [[1807.06209](#)].
- [9] H.-w. Zheng, F. Gao, L. Bian, S.-x. Qin and Y.-x. Liu, *Quantitative analysis of the gravitational wave spectrum sourced from a first-order chiral phase transition of QCD*, *Phys. Rev. D* **111** (2025) L021303 [[2407.03795](#)].
- [10] R. D. Pisarski and F. Wilczek, *Remarks on the Chiral Phase Transition in Chromodynamics*, *Phys. Rev. D* **29** (1984) 338.
- [11] F. R. Brown, F. P. Butler, H. Chen, N. H. Christ, Z.-h. Dong, W. Schaffer et al., *On the existence of a phase transition for QCD with three light quarks*, *Phys. Rev. Lett.* **65** (1990) 2491.
- [12] S. Resch, F. Rennecke and B.-J. Schaefer, *Mass sensitivity of the three-flavor chiral phase transition*, *Phys. Rev. D* **99** (2019) 076005 [[1712.07961](#)].
- [13] P. de Forcrand and M. D'Elia, *Continuum limit and universality of the Columbia plot*, *PoS LATTICE2016* (2017) 081 [[1702.00330](#)].
- [14] L. Dini, P. Hegde, F. Karsch, A. Lahiri, C. Schmidt and S. Sharma, *Chiral phase transition in three-flavor QCD from lattice QCD*, *Phys. Rev. D* **105** (2022) 034510 [[2111.12599](#)].
- [15] F. Cuteri, O. Philipsen and A. Sciarra, *On the order of the QCD chiral phase transition for different numbers of quark flavours*, *JHEP* **11** (2021) 141 [[2107.12739](#)].



- [16] G. Fejos, *Second-order chiral phase transition in three-flavor quantum chromodynamics?*, *Phys. Rev. D* **105** (2022) L071506 [2201.07909].
- [17] J. Bernhardt and C. S. Fischer, *QCD phase transitions in the light quark chiral limit*, *Phys. Rev. D* **108** (2023) 114018 [2309.06737].
- [18] A. Pasztor, *The QCD phase diagram at finite temperature and density - a lattice perspective*, *PoS LATTICE2023* (2024) 108.
- [19] J. P. Klinger, R. Kaiser and O. Philipsen, *The order of the chiral phase transition in massless many-flavour lattice QCD*, *PoS LATTICE2024* (2025) 172 [2501.19251].
- [20] V. Dick, F. Karsch, E. Laermann, S. Mukherjee and S. Sharma, *Microscopic origin of  $U_A(1)$  symmetry violation in the high temperature phase of QCD*, *Phys. Rev. D* **91** (2015) 094504 [1502.06190].
- [21] Y. Iwasaki, K. Kanaya, S. Kaya and T. Yoshie, *Scaling of chiral order parameter in two flavor QCD*, *Phys. Rev. Lett.* **78** (1997) 179 [hep-lat/9609022].
- [22] M. D'Elia, A. Di Giacomo and C. Pica, *On the order of the deconfining transition in  $N(f) = 2$  QCD*, *Int. J. Mod. Phys. A* **20** (2005) 4579 [hep-lat/0408011].
- [23] M. D'Elia, A. Di Giacomo and C. Pica, *Two flavor QCD and confinement*, *Phys. Rev. D* **72** (2005) 114510 [hep-lat/0503030].
- [24] J. B. Kogut and D. K. Sinclair, *Evidence for  $O(2)$  universality at the finite temperature transition for lattice QCD with 2 flavors of massless staggered quarks*, *Phys. Rev. D* **73** (2006) 074512 [hep-lat/0603021].
- [25] C. Bonati, P. de Forcrand, M. D'Elia, O. Philipsen and F. Sanfilippo, *Chiral phase transition in two-flavor QCD from an imaginary chemical potential*, *Phys. Rev. D* **90** (2014) 074030 [1408.5086].
- [26] O. Philipsen and C. Pinke, *The  $N_f = 2$  QCD chiral phase transition with Wilson fermions at zero and imaginary chemical potential*, *Phys. Rev. D* **93** (2016) 114507 [1602.06129].
- [27] F. Cuteri, O. Philipsen and A. Sciarra, *QCD chiral phase transition from noninteger numbers of flavors*, *Phys. Rev. D* **97** (2018) 114511 [1711.05658].
- [28] H. T. Ding, P. Hegde, F. Karsch, A. Lahiri, S. T. Li, S. Mukherjee et al., *Chiral phase transition of  $(2+1)$ -flavor QCD*, *Nucl. Phys. A* **982** (2019) 211 [1807.05727].
- [29] J. Braun, L. M. Haas, F. Marhauser and J. M. Pawłowski, *Phase Structure of Two-Flavor QCD at Finite Chemical Potential*, *Phys. Rev. Lett.* **106** (2011) 022002 [0908.0008].
- [30] J. Braun, W.-j. Fu, J. M. Pawłowski, F. Rennecke, D. Rosenblüh and S. Yin, *Chiral susceptibility in  $(2+1)$ -flavor QCD*, *Phys. Rev. D* **102** (2020) 056010 [2003.13112].
- [31] A. Bazavov, H. T. Ding, P. Hegde, F. Karsch, E. Laermann, S. Mukherjee et al., *Chiral phase structure of three flavor QCD at vanishing baryon number density*, *Phys. Rev. D* **95** (2017) 074505 [1701.03548].
- [32] Y. Kuramashi, Y. Nakamura, H. Ohno and S. Takeda, *Nature of the phase transition for finite temperature  $N_f = 3$  QCD with nonperturbatively  $O(a)$  improved Wilson fermions at  $N_t = 12$* , *Phys. Rev. D* **101** (2020) 054509 [2001.04398].
- [33] J. T. Lenaghan, *Influence of the  $U(1)_A$  anomaly on the QCD phase transition*, *Phys. Rev. D* **63** (2001) 037901 [hep-ph/0005330].
- [34] P. Kovacs and Z. Szep, *The critical surface of the  $SU(3)_L \times SU(3)_R$  chiral quark model at non-zero baryon density*, *Phys. Rev. D* **75** (2007) 025015 [hep-ph/0611208].
- [35] J. T. Lenaghan, D. H. Rischke and J. Schaffner-Bielich, *Chiral symmetry restoration at nonzero temperature in the  $SU(3)(r) \times SU(3)(l)$  linear sigma model*, *Phys. Rev. D* **62** (2000) 085008 [nucl-th/0004006].
- [36] K. Fukushima, *Phase diagrams in the three-flavor Nambu-Jona-Lasinio model with the Polyakov loop*, *Phys. Rev. D* **77** (2008) 114028 [0803.3318].
- [37] B.-J. Schaefer and M. Wagner, *The Three-flavor chiral phase structure in hot and dense QCD matter*, *Phys. Rev. D* **79** (2009) 014018 [0808.1491].
- [38] M. Mitter and B.-J. Schaefer, *Fluctuations and the axial anomaly with three quark flavors*, *Phys. Rev. D* **89** (2014) 054027 [1308.3176].
- [39] M. Grahl and D. H. Rischke, *Functional renormalization group study of the two-flavor linear sigma model in the presence of the axial anomaly*, *Phys. Rev. D* **88** (2013) 056014 [1307.2184].
- [40] J. Eser, M. Grahl and D. H. Rischke, *Functional Renormalization Group Study of the Chiral Phase Transition Including Vector and Axial-vector Mesons*, *Phys. Rev. D* **92** (2015) 096008 [1508.06928].
- [41] F. Giacosa, G. Kovács, P. Kovács, R. D. Pisarski and F. Rennecke, *Anomalous  $U(1)_A$  couplings and the Columbia plot*, *Phys. Rev. D* **111** (2025) 016014 [2410.08185].
- [42] G. Fejos and T. Hatsuda, *Order of the  $SU(N_f) \times SU(N_f)$  chiral transition via the functional renormalization group*, *Phys. Rev. D* **110** (2024) 016021 [2404.00554].
- [43] H. A. Ahmed, M. Kawaguchi and M. Huang, *Effect of charm quark on chiral phase transition in  $N_f=2+1+1$  holographic QCD*, *Phys. Rev. D* **110** (2024) 046002 [2401.04355].
- [44] G. Fejos and A. Patkos, *Thermal behavior of effective  $U_A(1)$  anomaly couplings in reflection of higher topological sectors*, *Phys. Rev. D* **109** (2024) 036035 [2311.02186].
- [45] R. D. Pisarski and F. Rennecke, *Conjectures about the Chiral Phase Transition in QCD from Anomalous Multi-Instanton Interactions*, *Phys. Rev. Lett.* **132** (2024) 251903 [2401.06130].
- [46] V. K. Tiwari, *Consistent chiral limit in the on-shell renormalized quark-meson model with ChPT scaling*, *Phys. Rev. D* **111** (2025) 114014 [2410.08461].
- [47] V. K. Tiwari, *Comparison of chiral limit studies in curvature mass versus on-shell renormalized quark-meson model using ChPT*, *2507.04597*.

- [48] A. Pilaftsis and D. Teresi, *Symmetry Improved CJT Effective Action*, *Nucl. Phys. B* **874** (2013) 594 [[1305.3221](#)].
- [49] H. Mao, *On the symmetry improved CJT formalism in the  $O(4)$  linear sigma model*, *Nucl. Phys. A* **925** (2014) 185 [[1305.4329](#)].
- [50] M. Kawaguchi, S. Matsuzaki and A. Tomiya, *Analysis of nonperturbative flavor violation at chiral crossover criticality in QCD*, *Phys. Rev. D* **103** (2021) 054034 [[2005.07003](#)].
- [51] Y. Kuroda, M. Harada, S. Matsuzaki and D. Jido, *Inverse Mass Hierarchy of Light Scalar Mesons Driven by Anomaly-Induced Flavor Breaking*, *PTEP* **2020** (2020) 053D02 [[1910.09146](#)].
- [52] J. M. Cornwall, R. Jackiw and E. Tomboulis, *Effective Action for Composite Operators*, *Phys. Rev. D* **10** (1974) 2428.
- [53] M. Kobayashi and T. Maskawa, *Chiral symmetry and eta-x mixing*, *Prog. Theor. Phys.* **44** (1970) 1422.
- [54] M. Kobayashi, H. Kondo and T. Maskawa, *Symmetry breaking of the chiral  $u(3) \times u(3)$  and the quark model*, *Prog. Theor. Phys.* **45** (1971) 1955.
- [55] G. 't Hooft, *Symmetry Breaking Through Bell-Jackiw Anomalies*, *Phys. Rev. Lett.* **37** (1976) 8.
- [56] G. 't Hooft, *Computation of the Quantum Effects Due to a Four-Dimensional Pseudoparticle*, *Phys. Rev. D* **14** (1976) 3432.
- [57] A. Gómez Nicola and J. Ruiz de Elvira, *Pseudoscalar susceptibilities and quark condensates: chiral restoration and lattice screening masses*, *JHEP* **03** (2016) 186 [[1602.01476](#)].
- [58] A. Gomez Nicola and J. Ruiz de Elvira, *Patterns and partners for chiral symmetry restoration*, *Phys. Rev. D* **97** (2018) 074016 [[1704.05036](#)].
- [59] G. Endrodi, Z. Fodor, S. D. Katz and K. K. Szabo, *The Nature of the finite temperature QCD transition as a function of the quark masses*, *PoS LATTICE2007* (2007) 182 [[0710.0998](#)].
- [60] K. Rajagopal and F. Wilczek, *Static and dynamic critical phenomena at a second order QCD phase transition*, *Nucl. Phys. B* **399** (1993) 395 [[hep-ph/9210253](#)].
- [61] M. Campostrini, A. Pelissetto, P. Rossi and E. Vicari, *25th order high temperature expansion results for three-dimensional Ising like systems on the simple cubic lattice*, *Phys. Rev. E* **65** (2002) 066127 [[cond-mat/0201180](#)].
- [62] M. Hasenbusch and T. Torok, *High precision Monte Carlo study of the 3-D XY universality class*, *J. Phys. A* **32** (1999) 6361 [[cond-mat/9904408](#)].